COUPLING STOKES FLOW WITH INHOMOGENEOUS POROELASTICITY

MATTEO TAFFETANI, RICARDO RUIZ-BAIER, AND SARAH WATERS

ABSTRACT. We investigate the behaviour of a system where a single phase fluid domain is coupled to a biphasic poroelastic domain. The fluid domain consists of an incompressible Newtonian viscous fluid while the poroelastic domain consists of a linear elastic solid filled with the same viscous fluid. The properties of the poroelastic domain, i.e. permeability and elastic parameters, depend on the inhomogeneous initial porosity field. The theoretical framework highlights how the heterogeneous material properties enter the linearised governing equations for the poroelastic domain. To couple flows through this domain with a surrounding Stokes flow, we show case a numerical implementation based on a new mixed formulation where the equations in the poroelastic domain are rewritten in terms of three fields: displacement, fluid pressure and total pressure.

Coupling single phase and multiphase flow problems are ubiquitous in many industrial and biological applications, and here we consider an example from in-vitro tissue engineering. We consider a perfusion system, where a flow is forced to pass from the single phase fluid to the biphasic poroelastic domain. We focus on a simplified two dimensional geometry with small aspect ratio, and perform an asymptotic analysis to derive analytical solutions for the displacement, the pressure and the velocity fields. Our analysis advances the quantitative understanding of the role of heterogeneous material properties of a poroelastic domain on its mechanics when coupled with a fluid domain. Specifically, (i) the analytical analysis gives closed form relations that can be directly used in the design of slender perfusion systems; (ii) the numerical method is validated by comparing its result against selected theoretical solutions, opening towards the possibility to investigate more complex geometrical configurations.

1. INTRODUCTION

In many biological and industrial applications, regions of poroelastic material are surrounded by a single-phase fluid. Examples include the soft permeable vessel walls that interface with the blood flow [1], the growth of an artificial poroelastic tissue within a perfusion bioreactor [2], the mechanics of bacteria biofilm placed in a surrounding fluid [3], and the processes of oil/gas extraction from fractured reservoirs [4].

In this paper, we provide fundamental insights into the understanding of the mechanical behaviour of these multiphase multiregion systems. We focus on a simplified setting where an incompressible Newtonian viscous fluid and a biphasic poroelastic material interact via conditions specified at their interface. The poroelastic domain consists of fluid and solid phases, both assumed intrinsically incompressible. The permeability and elastic properties of the poroelastic medium depend on the underlying porosity, which is assumed to be spatially varying.

The mechanics of a porous domain is usually described using the theory of mixtures [5] or the theory of poroelasticity [6]. These two approaches are equivalent in many contexts,

as in the analysis carried in this paper, but it is possible to highlight some fundamental differences. The theoretical framework underlying the former is suitable in the case of media with many constituents since the primary variables are the concentration and the velocity of each constituent. The latter is more straightforward when applied to biphasic media because the domain is seen as a composite material (or effective medium) having a fluid pressure and a solid displacement as primary variables. The pioneering works on biphasic poroelastic media developed by Terzaghi [7] and Biot [8] evaluated the simplest case where the domain undergoes small strains, and thus a linear elastic relation for the effective solid behaviour can be used, and the physical properties (the elastic parameters and the permeability) are constant and isotropic. Later works extended this approach to include kinematic nonlinearity [5, 9], constitutive nonlinearity in the description of the elastic phase and the use of nonlinear and anisotropic permeability field depending on the tortuosity of the porous network and the domain anisotropy [10–12]. There exist several levels of nonlinearity in the description of a poroelastic domain, i.e., kinematic (or geometrical), constitutive, or in the specification of the material properties once given the porosity field: for a comprehensive discussion we refer to [13] who address this issue in detail.

We extend the continuum framework for the poroelastic domain described above as follows. We investigate how the heterogeneous distribution of material properties affect the mechanical response of the system; here we assume that both the effective elastic parameters and the permeability have a nonlinear dependence on the porosity, that, in turn, depends on the spatial coordinates. The effect of the heterogeneity has been previously investigated using homogenisation techniques, where the upscaled equations that describe the mechanics of a heterogeneous poroelastic domain are formally derived once the presence of several separated scales is assumed [14, 15]. In comparison, our methodology provides more flexibility in choosing the spatial dependence of the material properties, as we are not constrained to a specific periodic pattern on the microscale. The interfacial conditions that describe the coupling between a fluid and a poroelastic domain are still a subject of ongoing research [16, 28, 29] and here we use the conditions proposed in [16] and adopted in [1].

We showcase our theoretical framework by specifying a geometrical setup consisting of a two-dimensional thin perfusion system where a fluid flow is forced to pass from a single phase fluid channel into a rectangular poroelastic domain (also known as consolidation problem). With our analytical solutions, we extend the work of [17] to the case of a deformable porous domain with heterogeneous properties, but limiting to the case of low Reynolds number, and we provide an analytical reference solution, later compared with our finite element solutions.

Recent applications of biphasic poroelasticity theory, e.g., in traumatic brain injuries [18], swelling of hydrogels [19], and cartilage biosynthesis [20], show the need for suitable numerical schemes that are able to solve consolidation problems in complex geometries. This requirement is even more urgent when the role of the interface is of importance since quantitative analytical advancement in the description of the interfacial zone is only possible in simplified settings [17]. A variety of finite element formulations exist for the coupling of incompressible fluid and poromechanics. For instance, partitioned formulations using either domain decomposition or Nitsche's approach can be found in [1, 21]; Lagrange-multiplier approaches for monolithic couplings have been recently addressed in [22]; and ghost penalty

methods have been employed for cut finite element methods valid in the regime of large deformations, in [23]. In the present work we propose a new mixed formulation where the poroelasticity equations are written using three fields (displacement, fluid pressure and total pressure, extending the ideas in [24, 25]). The main advantages of this method with respect to the existing approaches are that because of the structure of the weak forms the imposition of interface conditions does not require Lagrange multipliers across the interface; and also, that the formulation is robust with respect to the Lamé dilation modulus (so the convergence and stability remain valid independently of this parameter).

The paper is organised as follows. In section 2 we present the equations that govern the poroelastic domain, the fluid domain and the interfacial conditions. To obtain the governing equations for the small strain mechanics of a poroelastic domain with the permeability and both the shear and dilatation moduli dependent upon the porosity field, we re-derive the balance equations starting from the Eulerian description of the geometrical nonlinear mixture theory [13] and we point out where the non-uniform initial porosity enters the equations when written in the displacement – pressure formulation. We also highlight the key dimensionless parameters that govern the behaviour of the system. Section 3 is devoted to the derivation of the finite element scheme, including the variational form of the governing equations, the fully discrete problem in matrix form, and the formulation of a harmonic extension operator to deform the fluid domain. In section 4, we apply the mathematical framework to the specific problem of the perfusion in the thin two dimensional geometry. In this limit, we assume that the aspect ratio is small and in section 5 we are able to provide analytical relations that allows to characterise the system without solving the full fluid-poroelastic coupled problem numerically. In section 6 we select a set of geometrical and constitutive parameters to compare the analytical solution in the steady and oscillatory cases against the outcome of the finite element simulation to test the validity of the numerical method presented. We close with some remarks and possible extensions in section 7.

2. Governing equations

With reference to Fig. 2.1, we consider a spatial domain $\Omega \subset \mathbb{R}^d$, $d = 2, 3$, divided into subdomains Ω_F and Ω_P representing incompressible, viscous Newtonian fluid and poroelastic solid regions, respectively. The subdomain boundaries are $\partial \Omega_F$ and $\partial \Omega_P$, respectively. We denote the internal interface between the two subdomains by $\Sigma_i = \Omega_F \cap \Omega_P$ and the unit normal vector to the interface by $\boldsymbol{n}$, with the convention that the normal points from Ω_F to Ω_P. While Σ_i denotes internal interfaces, we denote the external boundaries of the subregions by $\Gamma_F = \partial \Omega_F \setminus \Sigma_i$ and $\Gamma_P = \partial \Omega_P \setminus \partial \Sigma_i$. Spatial coordinates are denoted by $\boldsymbol{x}$ while t denotes time.

We assume the fluid and solid constituents are intrinsically incompressible, i.e., the true densities are constant. We neglect gravitational and inertial effects throughout. We present the governing equations for the poroelastic domain (§2.1), the fluid domain (§2.2), and finally the interface conditions (§2.3). The equations and interfacial conditions are presented in dimensionless form, with the choice of nondimensionalisation motivated as follows. Throughout the system, we have an incompressible, viscous, Newtonian fluid with dynamic viscosity μ_f. The permeability of the poroelastic material to fluid is $\hat{\kappa}$. The dilation and shear moduli of the solid are of size $\hat{\mu}_s$, and we denote the characteristic displacement of the poroelastic material by δ. Assuming the spatial domain to have characteristic length L,
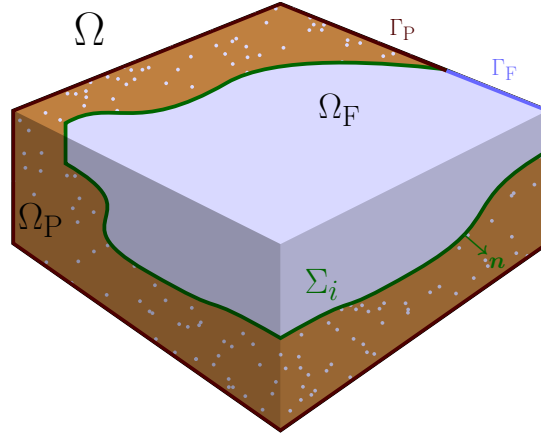
FIGURE 2.1. Schematic diagram of the multidomain configuration. The blue region is the fluid domain Ω_F; the brown region is the poroelastic domain Ω_P; the green curve is the interface Σ_i. The blue boundary represents Γ_F; and the purple boundary represents Γ_P.

the stresses in the poroelastic domain are of size $\hat{\mu}_s \delta / L$, and the size of the Darcy flows generated by gradients in stress are then $\hat{\kappa}\delta\hat{\mu}_s/(\mu_f L^2)$. The characteristic time τ is chosen to ensure the Darcy and solid skeleton velocities are comparable, i.e. that $\delta/\tau \sim \hat{\kappa}\delta\hat{\mu}_s/(\mu_f L^2)$, and so $\tau \sim (\mu_f L^2)/(\hat{\kappa}\hat{\mu}_s)$. Assuming flows of size U_{av} in the single-phase domain, the viscous pressure scale in given by $U_{av}\mu_f/L$.

2.1. **Poroelastic domain.** We derive the poroelastic equation starting from the framework of mixture theory. This enables us to highlight how additional physics commonly encountered in biological applications, e.g., mass transfer between constituent phases captured via additional terms in equations (2.2), may be incorporated in future model developments. The permeability and material properties (captured by the Lame constants of the solid) depend on the porosity, or equivalently the fluid volume fraction, of the poroelastic material. We consider the small strain limit, and reveal how spatial variations in the permeability and material properties of the poroelastic material enter the resulting governing equations.

The solid and fluid phases are indicated by subscripts s and f respectively, with corresponding volume fractions $\theta_s(\mathbf{x}, t)$ and $\theta_f(\mathbf{x}, t)$. We assume that at each point in space there are no voids so that

$$\theta_f + \theta_s = 1. \tag{2.1}$$

Assuming no mass transfer between the phases, the equations for conservation of mass and momentum for each phase are

$$\frac{\partial \theta_i}{\partial t} + \text{div}\,(\theta_i \boldsymbol{v}_i) = 0, \tag{2.2a}$$

$$\nabla \cdot (\theta_i \boldsymbol{\sigma}_i) + \sum_{j \neq i} \mathbf{m}_{ij} = 0, \tag{2.2b}$$

where $i, j \in \{s, f\}$, $\boldsymbol{v}_i(\boldsymbol{x}, t)$ is the velocity of phase i and $\mathbf{m}_{ij}(\boldsymbol{x}, t)$ defines the interphase momentum transfer. The stress tensor $\boldsymbol{\sigma}_i(\boldsymbol{x}, t)$ for each phase is decomposed into volumetric and deviatoric components as

$$\boldsymbol{\sigma}_f(\boldsymbol{x}, t) = -p_P\mathbf{I}, \tag{2.3a}$$

$$\boldsymbol{\sigma}_s(\boldsymbol{x}, t) = -p_P\mathbf{I} + \boldsymbol{\sigma}_s^*, \tag{2.3b}$$

where $p_P(\boldsymbol{x}, t)$ is the fluid pressure, $\mathbf{I}$ is the identity tensor, and $\boldsymbol{\sigma}_s^*(\boldsymbol{x}, t)$ is the elastic stress tensor due to deformations of the poroelastic material. Equation (2.3a) assumes that in the fluid phase the viscous effects are negligible compared to the hydrostatic contribution. The interphase momentum transfer terms are (see, e.g., [26])

$$\mathbf{m}_{ij} = p_P\nabla\theta_i + \Lambda(\boldsymbol{v}_j - \boldsymbol{v}_i), i, j \in \{f, s\}, \ i \neq j. \tag{2.4}$$

The second term on the right-hand side of equation (2.4) represents the viscous drag between the two phases, assumed proportional to the difference in velocity. The drag parameter can be defined in terms of the pore fluid viscosity μ_f and the permeability $\kappa(\theta_f)$ as $\Lambda = \theta_f^2\mu_f/\kappa$ [13, 26]. We rewrite the permeability as $\kappa(\theta) = \hat{\kappa}\mathcal{K}(\theta_f)$ where $\hat{\kappa}$ captures the size of the permeability and $\mathcal{K}$ is an $O(1)$ function reflecting the dependence of the permeability on the spatially varying fluid volume fraction.

Substituting (2.3a) into (2.2b), with $i = f$ in the latter, we obtain an expression for the Darcy velocity $\boldsymbol{v}_d(\boldsymbol{x}, t)$

$$\boldsymbol{v}_d = \theta_f(\boldsymbol{v}_f - \boldsymbol{v}_s) = -\frac{\hat{\kappa}\mathcal{K}}{\mu_f}\nabla p_P. \tag{2.5}$$

The velocity of the solid phase in terms of the solid phase displacement $\boldsymbol{d}(\boldsymbol{x}, t)$ is $\boldsymbol{v}_s(\boldsymbol{x}, t) = D\boldsymbol{d}/Dt = \partial\boldsymbol{d}/\partial t \cdot (\mathbf{I} + \nabla\boldsymbol{d})$. To describe the solid phase we introduce the effective stress $\boldsymbol{\sigma}'(\boldsymbol{x}, t) = \theta_s(\mathbf{x}, t)\boldsymbol{\sigma}_s^*(\boldsymbol{x}, t)$, known as Terzaghi stress [13] or drained stress [6], for which a constitutive relationship must be provided. Employing the no-void condition (2.1) to eliminate θ_s, and setting $\theta_f = \theta$ in the analysis that follows, the full nonlinear problem can be reduced to a system of three equations in three unknowns p_P, $\boldsymbol{d}$ and θ as

$$\nabla \cdot (\boldsymbol{\sigma}' - p_P\mathbf{I}) = \mathbf{0}, \tag{2.6a}$$

$$\frac{\partial\theta}{\partial t} + \nabla \cdot \left(-\frac{\hat{\kappa}\mathcal{K}}{\mu_f}\nabla p_P + \theta\frac{\partial\boldsymbol{d}}{\partial t} \cdot (\mathbf{I} + \nabla\boldsymbol{d})\right) = 0, \tag{2.6b}$$

$$-\frac{\partial\theta}{\partial t} + \nabla \cdot \left((1 - \theta)\frac{\partial\boldsymbol{d}}{\partial t} \cdot (\mathbf{I} + \nabla\boldsymbol{d})\right) = 0. \tag{2.6c}$$

Equation (2.6a) is the sum of the equilibrium equations of the two phases. Equations (2.6b) and (2.6c) are conservation of mass for the fluid and solid phases, respectively.

For simplicity, we introduce a linear constitutive relation for the Terzaghi stress tensor, given in dimensional form by

$$\boldsymbol{\sigma}'(\boldsymbol{x}, t) = 2\mu_s(\boldsymbol{x}, t)\boldsymbol{e}(\boldsymbol{d}) + \lambda(\boldsymbol{x}, t)(\nabla \cdot \boldsymbol{d})\mathbf{I}, \tag{2.7}$$

where $\boldsymbol{e}(\boldsymbol{d}) = (\nabla\boldsymbol{d} + \nabla\boldsymbol{d}^{\mathrm{t}})/2$ is the infinitesimal strain tensor and λ, μ_s are the Lamé constants of the solid (dilation and shear moduli, respectively), which we assume vary with the porosity via

$$\mu_s = \hat{\mu}_s\mathcal{H}(\theta), \quad \lambda = \hat{\mu}_s\mathcal{N}(\theta), \tag{2.8}$$

where $\hat{\mu}_s$ is constant, and $\mathcal{H}(\theta)$ and $\mathcal{N}(\theta)$ are $O(1)$ functions.

We now recast equations (2.6) and (2.7) in dimensionless form. Motivated by the discussion in §2, we non-dimensionalise as follows

$$\boldsymbol{x} = L\boldsymbol{X}, \quad \boldsymbol{d} = \delta\boldsymbol{D}, \quad t = \frac{\mu_f L^2}{\hat{\kappa}\hat{\mu}_s}T, \quad [\boldsymbol{\sigma}', p_p] = \frac{\hat{\mu}_s \delta}{L}[\boldsymbol{\Sigma}', P_P]. \tag{2.9}$$

Equations (2.6) in dimensionless form are

$$\nabla \cdot (\boldsymbol{\Sigma}' - P_P\mathbf{I}) = \mathbf{0}, \tag{2.10a}$$

$$\frac{\partial\theta}{\partial T} - \epsilon_L\nabla \cdot (\mathcal{K}(\theta)\nabla P_P) + \epsilon_L\nabla \cdot \left(\theta\frac{\partial\boldsymbol{D}}{\partial T}(\mathbf{I} + \epsilon_L\nabla\boldsymbol{D})\right) = 0, \tag{2.10b}$$

$$-\frac{\partial\theta}{\partial T} + \epsilon_L\nabla \cdot \left((1-\theta)\frac{\partial\boldsymbol{D}}{\partial T}(\mathbf{I} + \epsilon_L\nabla\boldsymbol{D})\right) = 0, \tag{2.10c}$$

$$\boldsymbol{\Sigma}' = 2\mathcal{H}(\theta)\boldsymbol{e}(\boldsymbol{D}) + \mathcal{N}(\theta)(\nabla \cdot \boldsymbol{D})\mathbf{I}. \tag{2.10d}$$

We consider the small strain limit, and expand all dependent variables as follows

$$\theta(\boldsymbol{X}, T) = \theta_0(\boldsymbol{X}, T) + \epsilon_L\theta_1(\boldsymbol{X}, T) + O(\epsilon_L^2), \tag{2.11}$$

with similar expansions for $P_P(\boldsymbol{X}, T)$, $\boldsymbol{D}(\boldsymbol{X}, T)$ and $\boldsymbol{\Sigma}'(\boldsymbol{X}, T)$. We also expand

$$\mathcal{K}(\theta) = \mathcal{K}_0(\theta_0(\boldsymbol{X}, T)) + O(\epsilon_L), \tag{2.12}$$

with similar expansions for $\mathcal{H}(\theta)$ and $\mathcal{N}(\theta)$. We substitute (2.11) and (2.12) into (2.10).

At leading order, equations (2.10b) and (2.10c) give $\theta_0(\boldsymbol{X}, T) = \theta^*(\boldsymbol{X})$ where $\theta^*(\boldsymbol{X})$ is the initial porosity distribution. From (2.12) the leading-order expansions of $\mathcal{K}$, $\mathcal{H}$ and $\mathcal{N}$ depends only on the initial porosity field $\theta^*(\boldsymbol{X})$, and in the remainder of the paper we reflect this dependence of $\mathcal{K}_0, \mathcal{H}_0$ and $\mathcal{N}_0$ on spatial coordinates $\boldsymbol{X}$ via the porosity distribution by writing $\mathcal{K}_0(\boldsymbol{X})$, $\mathcal{H}_0(\boldsymbol{X})$ and $\mathcal{N}_0(\boldsymbol{X})$.

At $O(\epsilon_L)$, equations (2.10) and (2.10d) read

$$\nabla \cdot (\boldsymbol{\Sigma}'_0 - P_{P,0}\mathbf{I}) = \mathbf{0}, \tag{2.13a}$$

$$\frac{\partial\theta_1}{\partial T} - \nabla \cdot (\mathcal{K}_0(\boldsymbol{X})\nabla P_{P,0}) + \nabla \cdot \left(\theta^*\frac{\partial\boldsymbol{D}_0}{\partial T}\right) = 0, \tag{2.13b}$$

$$-\frac{\partial\theta_1}{\partial T} + \nabla \cdot \left((1-\theta^*)\frac{\partial\boldsymbol{D}_0}{\partial T}\right) = 0, \tag{2.13c}$$

$$\boldsymbol{\Sigma}'_0 = 2\mathcal{H}_0(\boldsymbol{X})\boldsymbol{e}(\boldsymbol{D}_0) + \mathcal{N}_0(\boldsymbol{X})(\nabla \cdot \boldsymbol{D}_0)\mathbf{I}. \tag{2.13d}$$

From (2.13c) we obtain the relation between the variation of the fluid content and the solid displacement, and, assuming the displacement is zero initially, we find

$$\theta_1(\boldsymbol{X}, T) = \nabla \cdot ((1-\theta^*)\boldsymbol{D}_0). \tag{2.14}$$

Summing (2.13b) and (2.13c), and reintroducing for later convenience (see §4) the (dimensionless) Darcy velocity, $\boldsymbol{v}_d = (\hat{\kappa}\delta\hat{\mu}_s)/(\mu_f L^2)\mathbf{V}$, we obtain the following system

$$\nabla \cdot (\boldsymbol{\Sigma}' - P_P\mathbf{I}) = \mathbf{0}, \tag{2.15a}$$

$$\mathbf{V} = -\mathcal{K}_0(\mathbf{X})\nabla P_P, \tag{2.15b}$$

$$\nabla \cdot \left(\frac{\partial\boldsymbol{D}}{\partial T} + \mathbf{V}\right) = 0, \tag{2.15c}$$

$$\boldsymbol{\Sigma}' = 2\mathcal{H}_0(\boldsymbol{X})\boldsymbol{e}(\boldsymbol{D}) + \mathcal{N}_0(\boldsymbol{X})(\nabla \cdot \boldsymbol{D})\mathbf{I}, \tag{2.15d}$$

where $e(D) = (\nabla D + \nabla D^{\mathrm{t}})/2$, and we have dropped subscripts 0 in D, P_P and Σ'. We emphasise that the variation of porosity given by equation (2.14) decouples from equations (2.15), and can be computed *a posteriori*. The influence of the displacement on the permeability and elastic properties of the poroelastic material is present in the corrections $\mathcal{K}_1, \mathcal{H}_1, \mathcal{N}_1$, and this displacement effect does not enter the linearised formulation. This is consistent with [13], who argue against the use of deformation-dependent permeabilities in the context of geometrical and constitutive linear frameworks.

Our analysis reveals then influence of a heterogeneous initial fluid volume fraction, i.e., the initial porosity $\theta^*(X)$, on the mechanics of a linear poroelastic material. Focusing on equations (2.15) the initial porosity distribution enters only the functional form of $\mathcal{K}_0$, $\mathcal{H}_0$ and $\mathcal{N}_0$, while its spatial gradient enters in the variation of the fluid content given by (2.14). Equation (2.14) reveals how the pore structure is rearranged in response to deformation of the poroelastic material (captured via D). As an example, let us consider a solenoidal displacement field $\nabla \cdot D = 0$: in the case of a homogeneous initial porosity we necessarily have $\theta_1 = 0$, thus the porosity is unaffected; in the case of heterogeneous initial porosity, instead, this displacement causes a rearrangement of the pores of the form $\theta_1 = -\nabla \theta^* \cdot D$.

2.2. **Fluid domain.** In the single-phase domain, the fluid is governed by the Stokes and continuity equations. We let U_{av} denote the velocity scale, and non-dimensionalise the velocity via $u = U_{av}U$ and pressure via $p_f = (\mu_f U_{av}/L)P_F$. The dimensionless governing equations are then

$$-\nabla \cdot [2e(U) - P_F\mathbf{I}] = \mathbf{0}, \tag{2.16a}$$

$$\nabla \cdot U = 0. \tag{2.16b}$$

2.3. **Boundary and interfacial conditions.** To couple the equations in the poroelastic (2.15) and fluid (2.16) domains, we impose boundary and interfacial conditions. The boundary conditions are specific to the physical problem under consideration and we delay their specification until §4. For the interfacial conditions, we follow [1, 21], and impose continuity of normal fluxes of fluid, continuity of the traction, balance of the normal components of the stress in the fluid phase with the pressure in the porous domain, and the Beavers-Joseph-Saffman condition. In dimensional form, they are

$$u \cdot n = \left(\frac{\partial d}{\partial t} - \frac{\hat{\kappa}\mathcal{K}}{\mu_f}\nabla p_P\right) \cdot n, \tag{2.17a}$$

$$(2\mu_f e(u) - p_F\mathbf{I}) \cdot n = (\sigma' - p_P\mathbf{I}) \cdot n, \tag{2.17b}$$

$$-n \cdot [(2\mu_f e(u) - p_F\mathbf{I}) \cdot n] = p_P, \tag{2.17c}$$

$$-n \cdot [(2\mu_f e(u) - p_F\mathbf{I}) \cdot t] = \frac{\gamma \mu_f}{\sqrt{\hat{\kappa}\mathcal{K}}} \left(u - \frac{\partial d}{\partial t}\right) \cdot t, \tag{2.17d}$$

where $\gamma > 0$ is the slip coefficient, and we recall that the normal n on the interface is understood as pointing from the fluid domain Ω_F towards the porous structure Ω_P, while t denotes the tangent vector(s) to Σ_i (one tangent for the case of $d = 2$, and two tangent vectors normal to n for $d = 3$).

Non-dimensionalising as in sections §2.1 and 2.2, and retaining leading order terms in the asymptotic expansion as $\epsilon_L \to 0$, the interface conditions are

$$U_n \boldsymbol{U} \cdot \boldsymbol{n} = \left(\frac{\partial \boldsymbol{D}}{\partial T} - \mathcal{K}_0 \nabla P_P \right) \cdot \boldsymbol{n}, \tag{2.18a}$$

$$U_n K_n (2\boldsymbol{e}(\boldsymbol{U}) - P_F \mathbf{I}) \cdot \boldsymbol{n} = (\boldsymbol{\Sigma}' - P_P \mathbf{I}) \cdot \boldsymbol{n}, \tag{2.18b}$$

$$- U_n K_n \boldsymbol{n} \cdot (2\boldsymbol{e}(\boldsymbol{U}) - P_F \mathbf{I}) \cdot \boldsymbol{n} = P_P, \tag{2.18c}$$

$$- U_n \boldsymbol{n} \cdot (2\boldsymbol{e}(\boldsymbol{U}) - P_F \mathbf{I}) \cdot \boldsymbol{t} = \frac{\gamma}{\sqrt{K_n \mathcal{K}_0}} \left(U_n \boldsymbol{U} - \frac{\partial \boldsymbol{D}}{\partial T} \right) \cdot \boldsymbol{t}, \tag{2.18d}$$

where $K_n = \hat{\kappa}/L^2$ is the ratio between the area occupied by the pores and the characteristic cross section L^2 of the poroelastic domain [17], $U_n = U_{av} \mu_f L^2 / (\delta \hat{\mu}_s \hat{\kappa})$ is the ratio of velocity scales in the Stokes and poroelastic domains, and $K_n U_n$ captures the ratio between pressure scales in the Stokes and Darcy domains.

3. Finite element computations - weak formulation and Galerkin method

To derive a finite element scheme we first state a weak form of the governing equations. We introduce the *total pressure* $\varphi = p_P - \lambda \nabla \cdot \boldsymbol{d}$ (following [24,25]) and the dimensional version of the problem in Ω_P described by (2.15) is restated in terms of the solid displacement $\boldsymbol{d}$, the fluid pressure p_P, and the total pressure φ, as

$$- \nabla \cdot (2\hat{\mu}_s \mathcal{H} \boldsymbol{e}(\boldsymbol{d}) - \varphi \mathbf{I}) = \boldsymbol{0}, \tag{3.1a}$$

$$\varphi - p_P + \hat{\mu}_s \mathcal{N} (\nabla \cdot \boldsymbol{d}) = 0, \tag{3.1b}$$

$$\frac{1}{\lambda} \frac{\partial p_P}{\partial t} - \frac{1}{\lambda} \frac{\partial \varphi}{\partial t} - \nabla \cdot \left(\frac{\hat{\kappa} \mathcal{K}}{\mu_f} \nabla p_P \right) = 0. \tag{3.1c}$$

After testing (3.1a)-(3.1c), together with the continuity and Stokes equations in the fluid domain, against suitable smooth functions $\boldsymbol{v}_F, q_F, \boldsymbol{w}, q_P, \psi$, we apply integration by parts wherever adequate. Then, proceeding similarly as in, e.g., [30], using the interfacial conditions (2.17a)–(2.17d), we arrive at the following remainder on the interface

$$I_{\Sigma_i} = \langle p_P, (\boldsymbol{v}_F - \boldsymbol{w}) \cdot \boldsymbol{n} \rangle_{\Sigma_i} + \langle \frac{\gamma \mu_f}{\sqrt{\hat{\kappa} \mathcal{K}}} (\boldsymbol{u}_F - \frac{\partial \boldsymbol{d}}{\partial t}) \cdot \boldsymbol{t}, (\boldsymbol{v}_F - \boldsymbol{w}) \cdot \boldsymbol{t} \rangle_{\Sigma_i} - \langle (\boldsymbol{u}_F - \frac{\partial \boldsymbol{d}}{\partial t}) \cdot \boldsymbol{n}, q_P \rangle_{\Sigma_i}, \tag{3.2}$$

where $\langle \cdot, \cdot \rangle_{\Sigma_i}$ denotes the pairing between the trace functional space $H^{1/2}(\Sigma_i)$ and its dual $H^{-1/2}(\Sigma_i)$. To keep the formulation general, we call $\Gamma_F^{\boldsymbol{u}_F}$ the part of the boundary of the single fluid domain such that $\boldsymbol{u}_F = \boldsymbol{0}$, $\Gamma_P^{\boldsymbol{d}}$ the part of the boundary of the poroelastic domain such that $\boldsymbol{d} = \boldsymbol{0}$ and $\Gamma_P^{p_P}$ the part of the boundary of the poroelastic domain such that $p_P = 0$. Accordingly, we consider the Sobolev spaces

$$\mathbf{H}_\star^1(\Omega_F) = \{\boldsymbol{v}_F \in \mathbf{H}^1(\Omega_F) : \boldsymbol{v}_F|_{\Gamma_F^{\boldsymbol{u}_F}} = \boldsymbol{0}\}, \quad \mathbf{H}_\star^1(\Omega_P) = \{\boldsymbol{w} \in \mathbf{H}^1(\Omega_P) : \boldsymbol{w}|_{\Gamma_P^{\boldsymbol{d}}} = \boldsymbol{0}\},$$

$$H_\star^1(\Omega_P) = \{q_P \in H^1(\Omega_P) : q_P|_{\Gamma_P^{p_P}} = 0\}, \tag{3.3}$$

and consequently we have the following mixed variational form: For a fixed $t > 0$, find $\boldsymbol{u}_F \in \mathbf{H}_\star^1(\Omega_F)$, $p_F \in L^2(\Omega_F)$, $\boldsymbol{d} \in \mathbf{H}_\star^1(\Omega_P)$, $p_P \in H_\star^1(\Omega_P)$, $\varphi \in L^2(\Omega_P)$, such that

$$a_2^F(\boldsymbol{u}_F, \boldsymbol{v}_F) + a_3^{\Sigma_i}(\boldsymbol{u}_F, \boldsymbol{v}_F) + b_1^F(\boldsymbol{v}_F, p_F) + b_2^{\Sigma_i}(\boldsymbol{v}_F, p_P) + b_3^{\Sigma_i}(\boldsymbol{v}_F, \frac{\partial \boldsymbol{d}}{\partial t}) = 0 \quad \forall \boldsymbol{v}_F \in \mathbf{H}_\star^1(\Omega_F),$$

$$b_1^F(\boldsymbol{u}_F, q_F) = 0 \quad \forall q_F \in L^2(\Omega_F),$$

$$b_3^{\Sigma_i}(\boldsymbol{u}_F, \boldsymbol{w}) + \tilde{\alpha} b_4^{\Sigma_i}(\boldsymbol{w}, p_P) + a_4^P(\boldsymbol{d}, \boldsymbol{w}) + a_5^{\Sigma_i}(\frac{\partial \boldsymbol{d}}{\partial t}, \boldsymbol{w}) + b_5^P(\boldsymbol{w}, \varphi) = 0 \quad \forall \boldsymbol{w} \in \mathbf{H}_\star^1(\Omega_P),$$

(3.4)

$$b_2^{\Sigma_i}(\boldsymbol{u}_F, q_P) + b_4^{\Sigma_i}(\frac{\partial \boldsymbol{d}}{\partial t}, q_P) + a_6^P(\frac{\partial p_P}{\partial t}, q_P) + a_7^P(p_P, q_P) - b_6^P(\frac{\partial \varphi}{\partial t}, q_P) = 0 \quad \forall q_P \in H_\star^1(\Omega_P),$$

$$b_5^P(\boldsymbol{d}, \psi) + b_6^P(\psi, p_P) - a_3^P(\varphi, \psi) = 0 \quad \forall \psi \in L^2(\Omega_P),$$

where the variational forms and linear functionals are defined as

$$a_2^F(\boldsymbol{u}_F, \boldsymbol{v}_F) = \int_{\Omega_F} 2\mu_f \boldsymbol{e}(\boldsymbol{u}_F) : \boldsymbol{e}(\boldsymbol{v}_F), \quad a_3^{\Sigma_i}(\boldsymbol{u}_F, \boldsymbol{v}_F) = \langle \frac{\gamma \mu_f}{\sqrt{\hat{\kappa}\mathcal{K}}} \boldsymbol{u}_F \cdot \boldsymbol{t}, \boldsymbol{v}_F \cdot \boldsymbol{t} \rangle_{\Sigma_i},$$

$$b_1^F(\boldsymbol{v}_F, q_F) = -\int_{\Omega_F} q_F \operatorname{div} \boldsymbol{v}_F, \quad b_2^{\Sigma_i}(\boldsymbol{v}_F, q_P) = \langle q_P, \boldsymbol{v}_F \cdot \boldsymbol{n} \rangle_{\Sigma_i}, \quad b_3^{\Sigma_i}(\boldsymbol{v}_F, \boldsymbol{d}) = -\langle \frac{\gamma \mu_f}{\sqrt{\hat{\kappa}\mathcal{K}}} \boldsymbol{v}_F \cdot \boldsymbol{t}, \boldsymbol{d} \cdot \boldsymbol{t} \rangle_{\Sigma_i},$$

$$b_4^{\Sigma_i}(\boldsymbol{w}, q_P) = -\langle q_P, \boldsymbol{w} \cdot \boldsymbol{n} \rangle_{\Sigma_i}, \quad a_4^P(\boldsymbol{d}, \boldsymbol{w}) = \int_{\Omega_P} 2\hat{\mu}_s \mathcal{H} \boldsymbol{e}(\boldsymbol{d}) : \boldsymbol{e}(\boldsymbol{w}),$$

(3.5)

$$a_5^{\Sigma_i}(\boldsymbol{d}, \boldsymbol{w}) = \langle \frac{\gamma \mu_f}{\sqrt{\hat{\kappa}\mathcal{K}}} \boldsymbol{d} \cdot \boldsymbol{t}, \boldsymbol{w} \cdot \boldsymbol{t} \rangle_{\Sigma_i}, \quad b_5^P(\boldsymbol{w}, \psi) = -\int_{\Omega_P} \psi \operatorname{div} \boldsymbol{w}, \quad a_6^P(p_P, q_P) = \int_{\Omega_P} \frac{1}{\hat{\mu}_s \mathcal{N}} p_P q_P,$$

$$a_7^P(p_P, q_P) = \int_{\Omega_P} \frac{\hat{\kappa}\mathcal{K}}{\mu_f} \nabla p_P \cdot \nabla q_P, \quad b_6^P(\psi, q_P) = \int_{\Omega_P} \frac{1}{\hat{\mu}_s \mathcal{N}} \psi q_P, \quad a_3^P(\varphi, \psi) = \int_{\Omega_P} \frac{1}{\hat{\mu}_s \mathcal{N}} \varphi \psi.$$

Note that we did not require additional Lagrange multipliers to enforce the interfacial conditions between the fluid and poroelastic sub-problems, since the functional spaces (3.3) indicate that pressure, velocity, and displacement traces (and also the traces of the corresponding test functions) appearing in (3.2) are all well-defined.

Regarding the finite element discretisation, as usual we denote by $\mathcal{T}_h$ a shape-regular simplicial mesh for the domain $\bar{\Omega}$ conformed by elements of maximal diameter h. If we denote by $\mathbb{P}_k(S)$ the space of polynomial functions defined locally on S and being of total degree up to k, then the finite-dimensional spaces characterising the discrete problem are

$$\mathbf{V}_h := \{\boldsymbol{v}_{F,h} \in \mathbf{C}(\overline{\Omega_F}) \cap \mathbf{H}_\star^1(\Omega_F) : \boldsymbol{v}_{F,h}|_K \in \mathbb{P}_{k+1}(K)^d, \ \forall K \in \mathcal{T}_h\},$$

$$Q_h^F := \{q_{F,h} \in \mathrm{C}(\overline{\Omega_F}) : q_{F,h}|_K \in \mathbb{P}_k(K), \ \forall K \in \mathcal{T}_h\},$$

(3.6)

$$\mathbf{W}_h := \{\boldsymbol{w}_h \in \mathbf{C}(\overline{\Omega_P}) \cap \mathbf{H}_\star^1(\Omega_P) : \boldsymbol{w}_h|_K \in \mathbb{P}_{k+1}(K)^d, \ \forall K \in \mathcal{T}_h\},$$

(3.7)

$$Q_h^P := \{q_{P,h} \in \mathrm{C}(\overline{\Omega_F}) \cap H_\star^1(\Omega_P) : q_{P,h}|_K \in \mathbb{P}_k(K), \ \forall K \in \mathcal{T}_h\},$$

(3.8)

$$Z_h := \{\psi_h \in \mathrm{L}^2(\Omega_P) : \psi_h|_K \in \mathbb{P}_k(K), \ \forall K \in \mathcal{T}_h\}.$$

(3.9)

We apply a time semi-discretisation of (3.4) using backward Euler's method with fixed time step Δt, and then starting from initial data, at each time iteration $n = 1, \ldots$, we look for $(\boldsymbol{u}_{F,h}^{n+1}, p_{F,h}^{n+1}, \boldsymbol{d}_h^{n+1}, p_{P,h}^{n+1}, \varphi_h^{n+1}) \in \mathbf{V}_h \times Q_h^F \times \mathbf{W}_h \times Q_h^P \times Z_h$ such that

$$\begin{bmatrix} \mathcal{A}_2^F + \mathcal{A}_3^\Sigma & (\mathcal{B}_1^F)' & \frac{1}{\Delta t}(\mathcal{B}_3^\Sigma)' & \tilde{\alpha}(\mathcal{B}_2^\Sigma)' & \mathbf{0} \\ \mathcal{B}_1^F & \mathbf{0} & \mathbf{0} & \mathbf{0} & \mathbf{0} \\ \mathcal{B}_3^\Sigma & \mathbf{0} & \mathcal{A}_4^P + \frac{1}{\Delta t}\mathcal{A}_5^\Sigma & \tilde{\alpha}(\mathcal{B}_4^\Sigma)' & (\mathcal{B}_5^P)' \\ \mathcal{B}_2^\Sigma & \mathbf{0} & \frac{1}{\Delta t}\mathcal{B}_4^\Sigma & \frac{1}{\Delta t}\mathcal{A}_6^P + \mathcal{A}_7^P & -\frac{1}{\Delta t}(\mathcal{B}_6^P)' \\ \mathbf{0} & \mathbf{0} & \mathcal{B}_5^P & \mathcal{B}_6^P & -\mathcal{A}_3^P \end{bmatrix} \begin{bmatrix} \boldsymbol{u}_{F,h}^{n+1} \\ p_{F,h}^{n+1} \\ \boldsymbol{d}_h^{n+1} \\ p_{P,h}^{n+1} \\ \varphi_h^{n+1} \end{bmatrix}$$
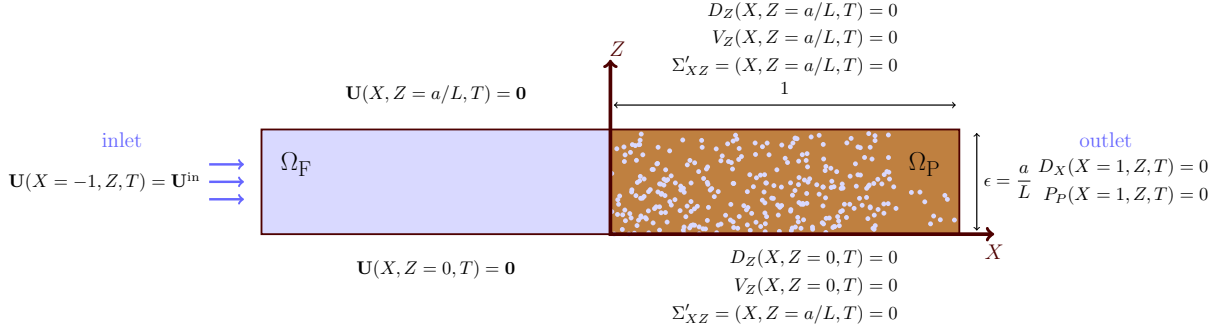
$$D_Z(X, Z = a/L, T) = 0$$
$$V_Z(X, Z = a/L, T) = 0$$
$$\Sigma'_{XZ} = (X, Z = a/L, T) = 0$$

$$\mathbf{U}(X, Z = a/L, T) = \mathbf{0}$$

inlet

$$\mathbf{U}(X = -1, Z, T) = \mathbf{U}^{\mathrm{in}}$$

$$\Omega_{\mathrm{F}}$$

$$\Omega_{\mathrm{P}}$$

outlet

$$\epsilon = \frac{a}{L} \quad \begin{array}{l} D_X(X = 1, Z, T) = 0 \\ P_P(X = 1, Z, T) = 0 \end{array}$$

$$\mathbf{U}(X, Z = 0, T) = \mathbf{0}$$

$$D_Z(X, Z = 0, T) = 0$$
$$V_Z(X, Z = 0, T) = 0$$
$$\Sigma'_{XZ} = (X, Z = a/L, T) = 0$$

FIGURE 4.1. Sketch of the two-dimensional channel geometry in rescaled variables, indicating the single-phase fluid and poroelastic regions, together with the boundary conditions.

$$= \begin{bmatrix} \frac{1}{\Delta t}(\mathcal{B}_3^{\Sigma})' \boldsymbol{d}_h^n \\ \mathbf{0} \\ \frac{1}{\Delta t}\mathcal{A}_5^{\Sigma} \boldsymbol{d}_h^n \\ \frac{1}{\Delta t}\mathcal{B}_4^{\Sigma} \boldsymbol{d}_h^n + \frac{1}{\Delta t}\mathcal{A}_6^P p_{P,h}^n - \frac{1}{\Delta t}(\mathcal{B}_6^P)' \varphi_h^n \\ \mathbf{0} \end{bmatrix}, \tag{3.10}$$

where the operators in calligraphic letters from (3.10) are induced by the variational forms in (3.5), and the $(\cdot)'$ denotes the dual operator resulting in the transpose block matrix of a given elementary block.

All routines have been implemented using the open source finite element library `FEniCS` [31], as well as the specialised module `multiphenics` (mathlab.sissa.it/multiphenics) for handling subdomain- and boundary- restricted terms that we require to impose interfacial conditions across interfaces. The polynomial degree employed for the simulations is $k = 1$.

4. PERFUSION IN A THIN TWO-DIMENSIONAL GEOMETRY

We now apply the framework detailed in §2 to a two-dimensional channel where the flow is forced to pass through a single-phase fluid region into a poroelastic domain. The governing equations are solved analytically in §5. We show how deformability and heterogeneity affect the flow through the system, and compare the obtained solutions with simplified scenarios corresponding to (*i*) a steady upstream velocity, (*ii*) a rigid solid skeleton, and (*iii*) homogeneous porosity distribution. In §6, the governing equations are solved numerically (using the finite-element approach described in §3) and the numerical method is validated against selected asymptotic solutions obtained in §5.

The problem setup (in dimensionless variables) is illustrated in Fig. 4.1. We consider a thin-channel, with width a small compared to the characteristic length L. We drive the flow via the specification of an upstream time-dependent velocity, and prescribe zero pressure and zero axial displacement at the outlet. We adopt a 2D Cartesian coordinate system $\boldsymbol{X} = (X, Z)$, where lengths are non-dimensionalised with respect to L. The corresponding coordinate directions are given by $\mathbf{e}_x$ and $\mathbf{e}_z$ respectively. We denote components of vectors via $\boldsymbol{U} = (U_X, U_Z)^{\mathrm{t}}$, $\boldsymbol{D} = (D_X, D_Z)^{\mathrm{t}}$, $\mathbf{V} = (V_X, V_Z)^{\mathrm{t}}$ and components of the stress tensor $\boldsymbol{\Sigma}'$ are denoted $\Sigma'_{XX}, \Sigma'_{XZ}$ and Σ'_{ZZ}.

The governing equations (2.15) and (2.16) are coupled via the interfacial conditions (2.18). Additionally, we specify the following boundary conditions. For the single-phase, fluid no-slip conditions are applied at the side walls $Z = 0, a/L$. In the poroelastic domain we impose zero transverse displacement, zero normal Darcy flow, and zero elastic shear stress at $Z = 0, a/L$. We prescribe a parabolic axial velocity profile $\boldsymbol{U}_{in}(X = -1, Z, T) = -6(U_{in}/U_{av})f(T)(Z^2 - Z)\mathbf{e}_x$ at the inlet $X = -1$, with $f(T)$ describing the time dependence of the imposed velocity profile, and $(U_{in}/U_{av})f(T)$ is the dimensionless inlet flux; in the steady case the time dependence reduces to $f(T) = 1$ while, in the oscillatory one, one can set $f(\Omega T)$ with $\Omega = \omega\left(\mu_f L^2/(\hat{\kappa}\hat{\mu}_s)\right)$ being the dimensionless pulsation (and ω the dimensional counterpart) of the forcing term. At the outlet $X = 1$, we prescribe $P_P(X = 1, Z, T) = 0$ and $D_X(X = 1, Z, T) = 0$, allowing the fluid to flow away from the poroelastic domain but the solid phase to be constrained. The undeformed interface is located at $X = 0$ and the unit normal and tangent vectors are $\boldsymbol{n} = \mathbf{e}_x$ and $\boldsymbol{t} = \mathbf{e}_z$.

We exploit the fact that the channel is thin, i.e., $a \ll L$, and introduce the small parameter $\epsilon = a/L$. The system is then characterised by the dimensionless parameters ϵ, K_n, U_n and U_{in}/U_{av}. Rewriting $K_n = \epsilon^2(\kappa/a^2)$ and requiring that $\bar{K} = \kappa/a^2$ is (at most) $O(1)$, we see that $K_n = \epsilon^2 \bar{K}$. Requiring the pressures in the single-phase fluid and poroelastic domains to be of the same size we see that $U_n K_n = O(1)$, and we set $U_n = \epsilon^{-2}$. To be consistent with the lubrication scalings given below in (5.1), we additionally choose $U_{in}/U_{av} = \epsilon^2$.

5. Analytical solution

We start by considering the governing equations (2.15) and (2.16) in the lubrication regime when the axial length scale ($O(1)$) is large compared with the transverse ($O(\epsilon)$) lengthscale. This assumption breaks down in inner regions either size of the interface (where the axial and transverse lengthscales are comparable). Following [17], we anticipate the presence of four regions, two outer domains of (dimensionless) length (1) (one fluid and one poroelastic) and two inner domains of dimensionless length ϵ (one fluid (domain I) and one poroelastic (domain IV)) as highlighted in Fig. 5.1. The interface conditions (2.18) are applied in the inner domain. We solve the system in the inner domains (one fluid (domain II) and one poroelastic (domain III)), consider their far field behaviour and match with the outer domain solutions, to derive conditions coupling the outer problems together. The asymptotic analysis is carried out to order $O(\epsilon)$ for two reasons: (i) the effect of porosity heterogeneities in the transverse direction appear at the order $O(\epsilon)$; and (ii) a complete description of the leading order behaviour in the inner regions requires information at $O(\epsilon)$ in the outer regions. Below we consider each domain separately.

5.1. **Asymptotic structure.**

5.1.1. *Outer domains I and IV.* In the outer domains, the axial length scale is large compared to the transverse lengthscale. We rescale as follows

$$(X, Z) = (\tilde{X}, \epsilon\tilde{Z}), \ (D_X, D_Z) = (\tilde{D}_X, \epsilon\tilde{D}_Z), \ (U_X, U_Z) = (\epsilon^2\tilde{U}_X, \epsilon^3\tilde{U}_Z),$$

$$(V_X, V_Z) = (\tilde{V}_X, \tilde{V}_Z), (P_F, P_P) = (\tilde{P}_F, \tilde{P}_P), \ (\Sigma'_{XX}, \Sigma'_{XZ}, \Sigma'_{ZZ}) = (\tilde{\Sigma}'_{XX}, \epsilon^{-1}\tilde{\Sigma}'_{XZ}, \tilde{\Sigma}'_{ZZ}).$$
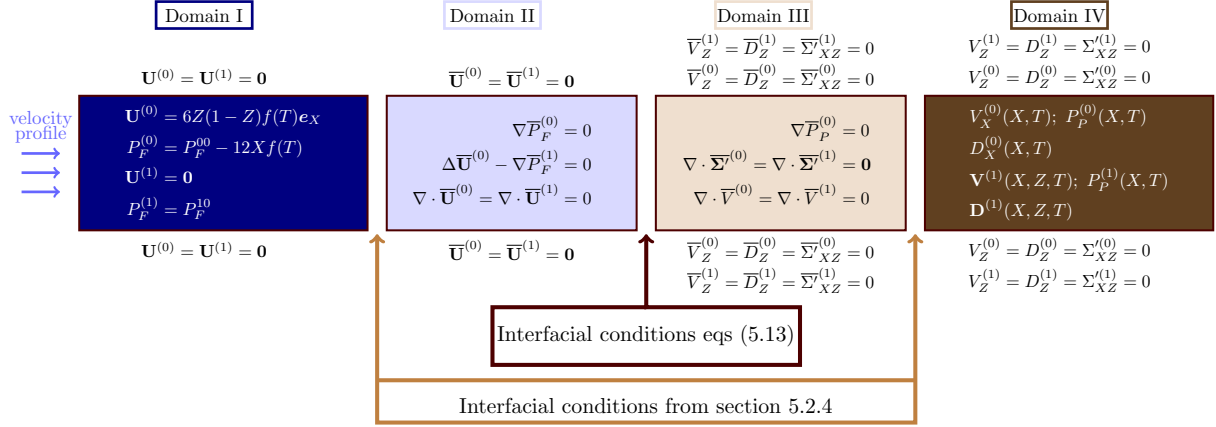
FIGURE 5.1. Sketch of asymptotic structure. The flow goes from left to right. Boxes I and II represent the fluid domain (outer - inner) while boxes III and IV are the poroelastic domain (inner - outer). The outer domains reduce to a Poiseuille - poroelastic system coupled through the interface conditions from §5.2.4. In the lubrication limit, the inner domains reduce to be a Stokes - rigid Darcy system with interface conditions derived in equations (5.11a)-(5.11d) decoupled with a divergence free stress field. Solution structures/governing equations are shown in the boxes.

Dropping the tildes, (2.15a), (2.15b) and (2.15c) in the poroelastic domain are now

$$\epsilon^2 \frac{\partial \Sigma'_{XX}}{\partial X} + \frac{\partial \Sigma'_{XZ}}{\partial Z} - \epsilon^2 \frac{\partial P_P}{\partial X} = 0, \quad \frac{\partial \Sigma'_{XZ}}{\partial X} + \frac{\partial \Sigma'_{ZZ}}{\partial Z} - \frac{\partial P_P}{\partial Z} = 0, \tag{5.1a}$$

$$V_X = -\mathcal{K}_0 \frac{\partial P_P}{\partial X}, \quad \epsilon^2 V_Z = -\mathcal{K}_0 \frac{\partial P_P}{\partial Z}, \tag{5.1b}$$

$$\frac{\partial}{\partial X}\left(\frac{\partial D_X}{\partial T} + V_X\right) + \frac{\partial}{\partial Z}\left(\frac{\partial D_Z}{\partial T} + V_Z\right) = 0, \tag{5.1c}$$

with the entries of the symmetric stress tensor $\mathbf{\Sigma}'$ specified as

$$\Sigma'_{XX} = 2\mathcal{H}_0 \frac{\partial D_X}{\partial X} + \mathcal{N}_0\left(\frac{\partial D_X}{\partial X} + \frac{\partial D_Z}{\partial Z}\right), \tag{5.2a}$$

$$\Sigma'_{ZZ} = 2\mathcal{H}_0 \frac{\partial D_Z}{\partial Z} + \mathcal{N}_0\left(\frac{\partial D_X}{\partial X} + \frac{\partial D_Z}{\partial Z}\right), \tag{5.2b}$$

$$\Sigma'_{XZ} = \mathcal{H}_0\left(\frac{\partial D_X}{\partial Z} + \epsilon^2 \frac{\partial D_Z}{\partial X}\right). \tag{5.2c}$$

The rescaled Stokes equations (2.16a) and (2.16b) are

$$\epsilon^2 \frac{\partial^2 U_X}{\partial X^2} + \frac{\partial^2 U_X}{\partial Z^2} - \frac{\partial P_F}{\partial X} = 0, \; \epsilon^4 \frac{\partial^2 U_Z}{\partial X^2} + \epsilon^2 \frac{\partial^2 U_Z}{\partial Z^2} - \frac{\partial P_F}{\partial Z} = 0, \tag{5.3a}$$

$$\frac{\partial U_X}{\partial X} + \frac{\partial U_Z}{\partial Z} = 0. \tag{5.3b}$$

The boundary conditions are

$$(U_X, U_Z) = (0,0) \quad \text{on} \quad Z = 0,1 \quad \text{for} \quad X < 0, \tag{5.4a}$$

$$(D_Z, V_Z, \Sigma'_{XZ}) = (0, 0, 0) \quad \text{on} \quad Z = 0, 1 \quad \text{for} \quad X > 0, \tag{5.4b}$$

$$D_X = 0, \quad P_P = 0 \quad \text{at} \quad X = 1, \tag{5.4c}$$

$$(U_X, U_Z) = (-6f(T)(Z^2 - Z), 0) \quad \text{at} \quad X = -1. \tag{5.4d}$$

We pose an asymptotic expansion, as $\epsilon \to 0$, of the form

$$
\begin{aligned}
(\boldsymbol{U}, P_F, \boldsymbol{D}, P_P, \mathbf{V}, \Sigma_{IJ}) &= \left(\boldsymbol{U}^{(0)}, P_F^{(0)}, \boldsymbol{D}^{(0)}, P_P^{(0)}, \mathbf{V}^{(0)}, \Sigma_{IJ}^{(0)} \right) \\
&+ \epsilon \left(\boldsymbol{U}^{(1)}, P_F^{(1)}, \boldsymbol{D}^{(1)}, P_P^{(1)}, \mathbf{V}^{(1)}, \Sigma_{IJ}^{(1)} \right) + O(\epsilon^2),
\end{aligned}
\tag{5.5}
$$

where $I, J \in X, Z$. The function $\mathcal{H}_0(X, \epsilon Z)$ is expanded as

$$\mathcal{H}_0(X, \epsilon Z) = \mathcal{H}_0^{(0)}(X) + \epsilon \left(\frac{\partial \mathcal{H}_0}{\partial \epsilon} \Big|_{\epsilon=0} \right) + O(\epsilon^2) = \mathcal{H}_0^{(0)}(X) + \epsilon \mathcal{H}_0^{(1)}(X, Z) + O(\epsilon^2), \tag{5.6}$$

and for $\mathcal{K}_0(X, \epsilon Z)$ and $\mathcal{N}_0(X, \epsilon Z)$ we proceed analogously. We note that the leading order fields are functions of X only.

5.1.2. *Inner domains II and III.* In the inner domains, the axial and transverse lengthscales are comparable, and we rescale as follows

$$(X, Z) = \epsilon(\bar{X}, \bar{Z}), \quad (D_X, D_Z) = (\bar{D}_X, \bar{D}_Z), \quad (U_X, U_Z) = (\epsilon^2 \bar{U}_X, \epsilon^2 \bar{U}_Z),$$

$$(V_X, V_Z) = (\bar{V}_X, \bar{V}_Z), \quad (\Sigma'_{XX}, \Sigma'_{XZ}, \Sigma'_{ZZ}) = \epsilon^{-1}(\bar{\Sigma}'_{XX}, \bar{\Sigma}'_{XZ}, \bar{\Sigma}'_{ZZ}).$$

We substitute these rescalings into (2.15) and (2.16), and define $\bar{\nabla} = (\partial/\partial\bar{X}, \partial/\partial\bar{Z})$.

In the inner fluid domain II we recover the scenario analysed in [17], and thus

$$-2\epsilon \bar{\nabla} \cdot \boldsymbol{e}(\bar{\boldsymbol{U}}) - \bar{\nabla} \bar{P}_F = \boldsymbol{0}, \qquad\qquad \nabla \cdot \bar{\boldsymbol{U}} = 0, \tag{5.7}$$

with $\boldsymbol{e}(\bar{\boldsymbol{U}}) = \left(\bar{\nabla}\bar{\boldsymbol{U}} + \bar{\nabla}\bar{\boldsymbol{U}}^t \right)/2$. In the inner porous domain III we have

$$\bar{\nabla} \cdot \left(\bar{\boldsymbol{\Sigma}}' - \epsilon \bar{P}_P \mathbf{I} \right) = \boldsymbol{0}, \qquad \epsilon \bar{\boldsymbol{V}} = -\mathcal{K}_0 \bar{\nabla} \bar{P}_P, \qquad \bar{\nabla} \cdot \left(\frac{\partial \bar{\boldsymbol{D}}}{\partial T} + \bar{\boldsymbol{V}} \right) = 0, \tag{5.8}$$

where the components of the symmetric solid stress in the porous domain $\bar{\boldsymbol{\Sigma}}'(\bar{\boldsymbol{X}}, T)$ are

$$\bar{\Sigma}'_{XX} = (2\mathcal{H}_0 + \mathcal{N}_0) \frac{\partial \bar{D}_X}{\partial \bar{X}} + \mathcal{N}_0 \frac{\partial \bar{D}_Z}{\partial \bar{Z}}, \tag{5.9a}$$

$$\bar{\Sigma}'_{ZZ} = (2\mathcal{H}_0 + \mathcal{N}_0) \frac{\partial \bar{D}_Z}{\partial \bar{Z}} + \mathcal{N}_0 \frac{\partial \bar{D}_X}{\partial \bar{X}}, \tag{5.9b}$$

$$\bar{\Sigma}'_{XZ} = \mathcal{H}_0 \left(\frac{\partial \bar{D}_Z}{\partial \bar{X}} + \frac{\partial \bar{D}_X}{\partial \bar{Z}} \right). \tag{5.9c}$$

At the top and the bottom boundaries, we have the boundary conditions

$$\bar{\boldsymbol{U}} = \boldsymbol{0} \quad \text{on} \quad \bar{Z} = 0, 1 \quad \text{for} \quad \bar{X} < 0, \tag{5.10a}$$

$$(\bar{D}_Z, \bar{V}_Z, \bar{\Sigma}'_{XZ}) = (0, 0, 0) \quad \text{on} \quad \bar{Z} = 0, 1 \quad \text{for} \quad \bar{X} > 0. \tag{5.10b}$$

The interface conditions (2.18a)–(2.18d) rescale as

$$\epsilon \bar{U}_X = \epsilon \frac{\partial \bar{D}_X}{\partial T} - \mathcal{K}_0 \frac{\partial \bar{P}_P}{\partial \bar{X}}, \tag{5.11a}$$

$$2\epsilon^2 \bar{K} \frac{\partial \bar{U}_X}{\partial \bar{X}} - \epsilon \bar{K} \bar{P}_F = \bar{\Sigma}'_{XX} - \epsilon \bar{P}_P; \epsilon^2 \bar{K} \frac{\partial \bar{U}_X}{\partial \bar{Z}} + \epsilon^2 \bar{K} \frac{\partial \bar{U}_Z}{\partial \bar{X}} = \bar{\Sigma}'_{XZ}, \quad (5.11b)$$

$$-2\epsilon \bar{K} \frac{\partial \bar{U}_X}{\partial \bar{X}} + \bar{K} \bar{P}_F = \bar{P}_P, \quad (5.11c)$$

$$\frac{\partial \bar{U}_X}{\partial \bar{Z}} + \frac{\partial \bar{U}_Z}{\partial \bar{X}} = \gamma \frac{1}{\sqrt{\bar{K}\mathcal{K}_0}} \left(\bar{U}_Z - \frac{\partial \bar{D}_Z}{\partial T} \right). \quad (5.11d)$$

In the inner domains, we pose an asymptotic expansion of the form

$$\left(\bar{\boldsymbol{U}}, \bar{P}_F, \bar{\boldsymbol{D}}, \bar{P}_P, \bar{\boldsymbol{V}} \right) = \left(\bar{\boldsymbol{U}}^{(0)}, \bar{P}_F^{(0)}, \bar{\boldsymbol{D}}^{(0)}, \bar{P}_P^{(0)}, \bar{\boldsymbol{V}}^{(0)} \right) + \epsilon \left(\bar{\boldsymbol{U}}^{(1)}, \bar{P}_F^{(1)}, \bar{\boldsymbol{D}}^{(1)}, \bar{P}_P^{(1)}, \bar{\boldsymbol{V}}^{(1)} \right) + O(\epsilon^2),$$
$$(5.12)$$

as $\epsilon \to 0$, and, consistently, the function $\mathcal{H}_0 \left(\bar{X}, \bar{Z} \right)$ is expanded as

$$\mathcal{H}_0 \left(\bar{X}, \bar{Z} \right) = \mathcal{H}_0^{(0)}(0) + \epsilon \left(\frac{\partial \mathcal{H}_0^{(0)} \left(\epsilon \bar{X} \right)}{\partial \epsilon} \Big|_{\epsilon=0} + \mathcal{H}_0^{(1)} \left(0, \bar{Z} \right) \right) + O(\epsilon^2), \quad (5.13)$$

and analogously for $\mathcal{K}_0 \left(\bar{X}, \bar{Z} \right)$ and $\mathcal{N}_0 \left(\bar{X}, \bar{Z} \right)$. Interestingly, the leading-order term of the material properties is constant in the inner porous domain.

In the following subsections, we present asymptotic solutions for the pressure, flow, deformation and stress fields in each of the regions I-IV, and show how coupling conditions can be derived from consideration of the inner solutions in regions II and III that match to the outer solutions in domains I and IV.

5.2. Asymptotic solution.

5.2.1. *Fluid domain I.* The behaviour in the outer fluid domain is analogous to the case studied in [17]. The leading and first-order solutions in domain I are (see Appendix A)

$$\boldsymbol{U}^{(0)} = 6Z(1-Z)f(T)\mathbf{e}_x, \qquad P_F^{(0)} = P_F^{00} - 12X f(T), \qquad (5.14a,b)$$

$$\boldsymbol{U}^{(1)} = \mathbf{0}, \qquad P_F^{(1)} = P_F^{10}(T). \qquad (5.14c,d)$$

Pressure splits into two unknowns P_F^{00} and $P_F^{10}(T)$: these will be determined via matching the leading and first-order pressure fields to the solutions in the inner domain (region II).

5.2.2. *Poroelastic domain IV.* The leading-order problem in domain IV reads

$$\frac{\partial \Sigma'^{(0)}_{XZ}}{\partial Z} = 0, \quad \frac{\partial \Sigma'^{(0)}_{XZ}}{\partial X} + \frac{\partial}{\partial Z} \left(\Sigma'^{(0)}_{ZZ} - P_P^{(0)} \right) = 0, \quad (5.15a,b)$$

$$V_X^{(0)} = -\mathcal{K}_0^{(0)}(X) \frac{\partial P_P^{(0)}}{\partial X}, \quad 0 = -\frac{\partial P_P^{(0)}}{\partial Z}, \quad (5.15c,d)$$

$$\frac{\partial}{\partial X} \left(\frac{\partial D_X^{(0)}}{\partial T} + V_X^{(0)} \right) + \frac{\partial}{\partial Z} \left(\frac{\partial D_Z^{(0)}}{\partial T} + V_Z^{(0)} \right) = 0, \quad (5.15e)$$

with

$$\Sigma'^{(0)}_{XZ} = \mathcal{H}_0^{(0)} \frac{\partial D_X^{(0)}}{\partial Z}, \quad \Sigma'^{(0)}_{ZZ} = \left(2\mathcal{H}_0^{(0)} + \mathcal{N}_0^{(0)} \right) \frac{\partial D_Z^{(0)}}{\partial Z} + \mathcal{N}_0^{(0)} \frac{\partial D_X^{(0)}}{\partial X}, \quad (5.16)$$

together with boundary conditions

$$\left(D_Z^{(0)}, V_Z^{(0)}, \Sigma'^{(0)}_{XZ} \right) = (0, 0, 0) \quad \text{on} \quad Z = 0, 1 \quad \text{for} \quad X > 0, \quad (5.17a)$$

$$D_X^{(0)} = 0, \quad P_P^{(0)} = 0 \quad \text{at} \quad X = 1. \tag{5.17b}$$

From equation (5.15c,d) we obtain

$$P_P^{(0)} = P_P^{(0)}(X,T), \quad V_X^{(0)} = -\mathcal{K}_0^{(0)} \frac{\partial P_P^{(0)}}{\partial X}. \tag{5.17a,b}$$

Equation (5.15e) subject to the condition $V_Z^{(0)}(X, Z = 0, T) = 0$ gives

$$V_Z^{(0)} = -\int_0^Z \frac{\partial}{\partial T} \left(\nabla \cdot \boldsymbol{D}^{(0)} \right) \mathrm{d}\zeta + Z \frac{\partial}{\partial X} \left(\mathcal{K}_0^{(0)} \frac{\partial P_P^{(0)}}{\partial X} \right). \tag{5.18}$$

Exploiting the boundary condition $V_Z^{(0)}(X, Z = 1, T) = 0$, together with the boundary condition $P_P^{(0)}(X = 1) = 0$ we obtain the following expression for the pressure

$$P_P^{(0)} = P_P^{01}(T) \int_1^X \frac{1}{\mathcal{K}_0^{(0)}} \mathrm{d}\xi + \int_1^X \frac{1}{\mathcal{K}_0^{(0)}} \left(\int_0^\xi \left(\int_0^1 \frac{\partial}{\partial T} \left(\nabla \cdot \boldsymbol{D}^{(0)} \right) \mathrm{d}\zeta \right) \mathrm{d}\eta \right) \mathrm{d}\xi. \tag{5.19}$$

The displacement and stress fields are computed from (5.15a,b) and (5.16), using the boundary conditions $D_Z^{(0)}(X, Z = 0, T) = D_Z^{(0)}(X, Z = 1, T)$ and $\Sigma_{XZ}^{\prime(0)}(X, Z = 0, T) = \Sigma_{XZ}^{\prime(0)}(X, Z = 1, T) = 0$. We find

$$\boldsymbol{D}^{(0)} = (A_D^{(0)}(X,T), 0), \ \Sigma_{XZ}^{\prime(0)} = 0, \ \Sigma_{ZZ}^{\prime(0)} = \mathcal{N}_0^{(0)} \partial D_X^{(0)} / \partial X. \tag{5.19a,b,c}$$

We see that the leading order fields are determined up to the specification of the functions $A_D^{(0)}(X,T)$, that depends on both the longitudinal coordinate X and the time T, and $P_P^{01}(T)$, that depends only on time T. We will discuss more about $A_D^{(0)}(X,T)$ later in this section while the condition to find the function $P_P^{01}(T)$ will be presented in §5.2.4 when matching the leading order velocity field against the solution in the inner region III.

The order $O(\epsilon)$ problem in domain IV reads

$$\frac{\partial \Sigma_{XZ}^{\prime(1)}}{\partial Z} = 0, \ \frac{\partial \Sigma_{ZZ}^{\prime(1)}}{\partial Z} - \frac{\partial P_P^{(1)}}{\partial Z} + \frac{\partial \Sigma_{XZ}^{\prime(1)}}{\partial X} = 0, \tag{5.20a,b}$$

$$V_X^{(1)} = -\left(\mathcal{K}_0^{(0)} \frac{\partial P_P^{(1)}}{\partial X} + \mathcal{K}_0^{(1)} \frac{\partial P_P^{(0)}}{\partial X} \right), \ 0 = -\frac{\partial P_P^{(1)}}{\partial Z}, \tag{5.20c,d}$$

$$\frac{\partial}{\partial X} \left(\frac{\partial D_X^{(1)}}{\partial T} + V_X^{(1)} \right) + \frac{\partial}{\partial Z} \left(\frac{\partial D_Z^{(1)}}{\partial T} + V_Z^{(1)} \right) = 0, \tag{5.20e}$$

with

$$\Sigma_{XZ}^{\prime(1)} = \mathcal{H}_0^{(0)} \frac{\partial D_X^{(1)}}{\partial Z} + \mathcal{H}_0^{(1)} \frac{\partial D_X^{(0)}}{\partial Z}, \tag{5.21}$$

$$\Sigma_{ZZ}^{\prime(1)} = \left(2\mathcal{H}_0^{(0)} + \mathcal{N}_0^{(0)} \right) \frac{\partial D_Z^{(1)}}{\partial Z} + \mathcal{N}_0^{(0)} \frac{\partial D_X^{(1)}}{\partial X} + \mathcal{N}_0^{(1)} \frac{\partial D_X^{(0)}}{\partial X}, \tag{5.22}$$

together with boundary conditions

$$(D_Z^{(1)}, V_Z^{(1)}, \Sigma_{XZ}^{\prime(1)}) = (0, 0, 0) \quad \text{on} \quad Z = 0, 1 \quad \text{for} \quad X > 0, \tag{5.23a}$$

$$D_X^{(1)} = 0, \quad P_P^{(1)} = 0 \quad \text{at} \quad X = 1. \tag{5.23b}$$

From equations (5.20c,d) we obtain

$$P_P^{(1)} = P_P^{(1)}(X,T), \quad V_X^{(1)} = -\left(\mathcal{K}_0^{(0)}\frac{\partial P_P^{(1)}}{\partial X} + \mathcal{K}_0^{(1)}\frac{\partial P_P^{(0)}}{\partial X}\right). \tag{5.23a,b}$$

Equation (5.20e) subject to the condition $V_Z^{(1)}(X, Z=0, T) = 0$ gives

$$V_Z^{(1)} = -\int_0^Z \frac{\partial}{\partial T}\left(\nabla \cdot \boldsymbol{D}^{(1)}\right)\mathrm{d}\zeta + \int_0^Z \frac{\partial}{\partial X}\left(\mathcal{K}_0^{(1)}\frac{\partial P_P^{(0)}}{\partial X}\right)\mathrm{d}\zeta + Z\frac{\partial}{\partial X}\left(\mathcal{K}_0^{(0)}\frac{\partial P_P^{(1)}}{\partial X}\right). \tag{5.24}$$

Exploiting the boundary condition $V_Z^{(1)}(X, Z=1, T) = 0$, together with the boundary condition $P_P^{(1)}(X=1) = 0$ we obtain the following expression for the pressure

$$P_P^{(1)} = P_P^{11}(T)\int_1^X \frac{1}{\mathcal{K}_0^{(0)}}\mathrm{d}\xi + \int_1^X \frac{1}{\mathcal{K}_0^{(0)}}\left(\int_0^\xi \left(G^{(1)}(\eta, T)\right)\mathrm{d}\eta\right)\mathrm{d}\xi. \tag{5.25}$$

with

$$G^{(1)} = \int_0^1 \frac{\partial}{\partial T}\left(\nabla \cdot \boldsymbol{D}^{(1)}\right)\mathrm{d}\zeta - \int_0^1 \frac{\partial}{\partial X}\left(\mathcal{K}_0^{(1)}\frac{\partial P_P^{(0)}}{\partial X}\right)\mathrm{d}\zeta. \tag{5.26}$$

The displacement and stress fields are computed from (5.20a,b) and (5.16), using the boundary conditions $D_Z^{(1)}(X, Z=0, T) = D_Z^{(1)}(X, Z=1, T)$ and $\Sigma_{XZ}'^{(1)}(X, Z=0, T) = \Sigma_{XZ}'^{(1)}(X, Z=1, T) = 0$. We find

$$\boldsymbol{D}^{(1)} = \left(A_D^{(1)}(X,T), \frac{1}{2\mathcal{H}_0^{(0)} + \mathcal{N}_0^{(0)}}\left(Z\int_0^1 \mathcal{N}_0^{(1)}\mathrm{d}\zeta - \int_0^Z \mathcal{N}_0^{(0)}\mathrm{d}\zeta\right)\frac{\partial A_D^{(0)}}{\partial X}\right),$$
$$\Sigma_{XZ}'^{(1)} = 0, \ \Sigma_{ZZ}'^{(1)} = \mathcal{N}_0^{(0)}\partial D_X^{(1)}/\partial X + \mathcal{N}_0^{(1)}\partial D_X^{(0)}/\partial X. \tag{5.26a,b,c}$$

The first-order fields are specified up to the unknown functions $A_D^{(0)}(X,T)$ and $P_P^{01}(T)$ already discussed about the leading order; in addition, they are determined up two other functions, $A_D^{(1)}(X,T)$ and $P_P^{11}(T)$. We will discuss more about $A_D^{(1)}(X,T)$ later in this section while the condition to find the function $P_P^{11}(T)$ will be presented in §5.2.4 when matching the first-order velocity field against the solution in the inner region III.

Before moving into the analysis of regions II and III, we determine the differential equations that must be satisfied by the functions $A_D^{(0)}(X,T)$ and $A_D^{(1)}(X,T)$. In domain IV we solve the equilibrium equation $\nabla \cdot (\boldsymbol{\Sigma}' - P_P\boldsymbol{I}) = 0$ (see equation (2.15a)). Denoting the area and boundary of the domain by $\mathcal{A}$ and $\mathcal{L}$, respectively, application of the divergence theorem to the square $[0, X] \times [0, 1]$ shown in Fig. 5.2 gives

$$\int_\mathcal{A} \nabla \cdot (\boldsymbol{\Sigma}' - P_P\boldsymbol{I})\,\mathrm{d}\mathcal{A} = \int_\mathcal{L} (\boldsymbol{\Sigma}' - P_P\boldsymbol{I})\cdot\boldsymbol{n}\mathrm{d}\mathcal{L} = \boldsymbol{0}, \tag{5.27}$$

where $\boldsymbol{n}$ is the unit outward normal vector to the boundary. Equation (5.27) then gives

$$\int_0^1 \left(-\left.(\Sigma_{XX}' - P_P)\right|_{X=0} + (\Sigma_{XX}' - P_P)\right)\mathrm{d}\zeta = -\frac{1}{\epsilon}\int_0^X \left(\left.\Sigma_{XZ}'\right|_{Z=1} - \left.\Sigma_{XZ}'\right|_{Z=0}\right)\mathrm{d}\xi = 0, \tag{5.28a}$$

$$\int_0^1 \left(-\left.\Sigma_{XZ}'\right|_{X=0} + \Sigma_{XZ}'\right)\mathrm{d}\zeta = -\epsilon\int_0^X \left(\left.(\Sigma_{ZZ}' - P_P)\right|_{Z=1} - \left.(\Sigma_{ZZ}' - P_P)\right|_{Z=0}\right)\mathrm{d}\xi. \tag{5.28b}$$

$$\boxed{\text{Domain IV}}$$

$$\begin{cases} \Sigma'_{ZZ}(X, Z = 1, T) \\ \Sigma'_{XZ}(X, Z = 1, T) & = 0 \\ P_P(X, T) \end{cases}$$

$$\begin{cases} \Sigma'_{XX}(X = 0, Z, T) & = \lim\limits_{\overline{X} \to \infty} \overline{\Sigma}_{XX} \\ \Sigma'_{XZ}(X = 0, Z, T) & = \lim\limits_{\overline{X} \to \infty} \overline{\Sigma}_{XZ} \\ P_P(X = 0, T) \end{cases} \qquad \nabla \cdot (\mathbf{\Sigma'} - P_P \mathbf{I}) = 0 \qquad \begin{cases} \Sigma'_{XX}(X, Z, T) \\ \Sigma'_{XZ}(X, Z, T) \\ P_P(X, T) \end{cases}$$

$$\begin{cases} \Sigma'_{ZZ}(X, Z = 0, T) \\ \Sigma'_{XZ}(X, Z = 0, T) & = 0 \\ P_P(X, T) \end{cases}$$

FIGURE 5.2. Structure of the elastic problem in term of stresses in the outer poroelastic domain IV. On the left of Domain IV, the conditions are derived matching with the inner solution on Domain III; on the top and bottom boundaries the conditions are obtained using the boundary conditions. On the right boundary we have the value for a generic coordinate X.

Equation (5.28a) at leading order gives

$$\Sigma'^{(0)}_{XX} - P^{(0)}_P = \Sigma'^{(0)}_{XX}(X = 0, T) - P^{(0)}_P(X = 0, T). \tag{5.29}$$

The relationship between stress and displacement (5.2a) gives an equation for $A^{(0)}_D(X, T)$

$$\left(2\mathcal{H}^{(0)}_0 + \mathcal{N}^{(0)}_0\right) \frac{\partial A^{(0)}_D}{\partial X} - P^{(0)}_P = \Sigma'^{(0)}_{XX}\big|_{X=0} - P^{(0)}_P(X = 0, T). \tag{5.30}$$

Equation (5.30) is solved subjected to the boundary condition $A^{(0)}_D(X = 1, T) = 0$. The function $\Sigma'^{(0)}_{XX}\big|_{X=0}(T)$ is unknown at this stage and it will be determined in §5.2.4 matching the leading order stress field to the solution obtained in the inner region III.

At $O(\epsilon)$ analogous arguments can be used to obtain an equation for $A^{(1)}_D$ as

$$\left(2\mathcal{H}^{(0)}_0 + \mathcal{N}^{(0)}_0\right) \frac{\partial A^{(1)}_D}{\partial X} + \frac{\partial A^{(0)}_D}{\partial X} \int_0^1 \left(2\mathcal{H}^{(1)}_0 + \mathcal{N}^{(1)}_0\right) \mathrm{d}\zeta - P^{(1)}_P = \Sigma'^{(1)}_{XX}\big|_{X=0} - P^{(1)}_P(X = 0, T). \tag{5.31}$$

Equation (5.31) is solved subjected to the boundary condition $A^{(1)}_D(X = 1, T) = 0$. The function $\Sigma'^{(1)}_{XX}\big|_{X=0}(T)$ is the last unknown that we have and it will be determined in §5.2.4 matching the first-order stress field with the solution obtained in the inner region III.

5.2.3. *Fluid domain II and Poroelastic domain III.* At leading order, the problems in the inner fluid domain (5.7) and in the inner poroelastic domain (5.8) coupled via (5.11) can be rearranged as follow. The leading-order pressure fields satisfy

$$\begin{cases} \bar{\nabla} \bar{P}^{(0)}_F = \mathbf{0}, & \text{in region II}, \\ \bar{\nabla} \bar{P}^{(0)}_P = \mathbf{0}, & \text{in region III}, \\ \bar{P}^{(0)}_P = \bar{K} \bar{P}^{(0)}_F & \text{on } \bar{X} = 0, \end{cases} \tag{5.32}$$

which gives that the pressures are constant and related via $\bar{P}^{(0)}_P = \bar{K} \bar{P}^{(0)}_F$.

The leading-order stress field in the poroelastic domain obeys

$$
\begin{cases}
\bar{\nabla} \cdot \bar{\boldsymbol{\Sigma}}'^{(0)} = \mathbf{0} & \text{in region III,} \\
\bar{\Sigma}_{XX}'^{(0)} = \bar{\Sigma}_{XZ}'^{(0)} = 0 & \text{on } \bar{X} = 0, \\
\bar{\Sigma}_{XZ}'^{(0)} = \bar{D}_Z^{(0)} = 0 & \text{on } \bar{Z} = 0, 1.
\end{cases}
\tag{5.33}
$$

We first note that $\bar{\Sigma}_{XX}'^{(0)}$ is symmetric with respect to $\bar{Z} = 0.5$. Applying the divergence theorem to equation (5.33)a in the domain $[0, \bar{X}] \times [0, 1]$, we find that $\int_0^1 \bar{\Sigma}_{XX}'^{(0)}(\bar{X}, Z, T) \mathrm{d}\zeta = 0$: thus $\bar{\Sigma}_{XX}'^{(0)} = 0$. If $\bar{\Sigma}_{XX}'^{(0)} = 0$, the axial component of (5.33)a, together with the boundary conditions $\bar{\Sigma}_{XZ}'^{(0)} = 0$ at $\bar{Z} = 0, 1$ gives that $\bar{\Sigma}_{XZ}'^{(0)} \equiv 0$. The transverse component of (5.33)a then gives $\bar{\Sigma}_{ZZ}'^{(0)} = h(\bar{X}, T)$. Having determined the form of the stress components, we use (5.9a) and (5.9b) to solve for the displacements: using the boundary condition $\bar{D}_Z^{(0)}(X, Z = 0, 1, T) = 0$, we get $\bar{D}_Z^{(0)} = 0$ (and $h(\bar{X}, T) = 0$) and $\bar{D}_X^{(0)} = g(\bar{Z}, T)$, i.e. $\bar{D}_X^{(0)}$ is independent by $\bar{X}$. Using (5.9c), $g(\bar{Z}, T) = g(T)$. The perhaps counterintuitive result is that the poroelastic inner region is stress-free and undergoes a rigid motion with $\bar{\boldsymbol{D}}^{(0)} = \left(\bar{D}_X^{(0)}(T), 0 \right)$.

At $O(\epsilon)$ equations (5.7) and (5.8), coupled via (5.11), reveal that the elastic problem decouples from the fluid flow at this order, and we can solve (i) an elastic problem for $\bar{\boldsymbol{D}}^{(1)}$ valid in region III only and (ii) a Stokes-Darcy problem in the unknowns $\left(\bar{P}_F^{(1)}, \bar{\boldsymbol{U}}^{(0)}, \bar{P}_P^{(1)} \right)$ in regions II and III.

The elastic problem is

$$
\begin{cases}
\bar{\nabla} \cdot \bar{\boldsymbol{\Sigma}}'^{(1)} = \mathbf{0} & \text{in region III,} \\
\bar{\Sigma}_{XX}'^{(1)} = \bar{P}_P^{(0)} - \bar{K} \bar{P}_F^{(0)}, \quad \bar{\Sigma}_{XZ}'^{(1)} = 0 & \text{on } \bar{X} = 0, \\
\bar{\Sigma}_{XZ}'^{(1)} = \bar{D}_Z^{(1)} = 0 & \text{on } \bar{Z} = 0, 1.
\end{cases}
\tag{5.34}
$$

Recalling that $\bar{P}_P^{(0)} - \bar{K} \bar{P}_F^{(0)} = 0$ at $\bar{X} = 0$ (see equation 5.32c), we can repeats the arguments made at leading order to show that at this order the poroelastic domain is again stress-free and undergoes a displacement $\bar{\boldsymbol{D}}^{(1)} = \left(\bar{D}_X^{(1)}(T), 0 \right)$.

The coupled Stokes-Darcy problem is

$$
\begin{cases}
\nabla^2 \bar{\boldsymbol{U}}^{(0)} - \nabla \bar{P}_F^{(1)} = \mathbf{0} \quad \text{and} \quad \nabla \cdot \bar{\boldsymbol{U}}^{(0)} = 0, & \text{in region II,} \\
\bar{\boldsymbol{V}}^{(0)} = -\mathcal{K}_0^{(0)}(0) \nabla \bar{P}_P^{(1)} \quad \text{and} \quad \nabla \cdot \bar{\boldsymbol{V}}^{(0)} = 0, & \text{in region III,} \\
\bar{U}_X^{(0)} = \dfrac{\partial \bar{D}_X^{(0)}}{\partial T} - \mathcal{K}_0^{(0)}(0) \dfrac{\partial \bar{P}_P^{(1)}}{\partial X}, & \text{on } \bar{X} = 0, \\
\bar{P}_P^{(1)} = \bar{K} \bar{P}_F^{(1)} - 2\bar{K} \dfrac{\partial \bar{U}_X^{(0)}}{\partial X}, & \text{on } \bar{X} = 0, \\
\dfrac{\partial \bar{U}_X^{(0)}}{\partial Z} + \dfrac{\partial \bar{U}_Z^{(0)}}{\partial X} = \gamma \dfrac{1}{\sqrt{\bar{K} \mathcal{K}_0^{(0)}(0)}} \bar{U}_Z^{(0)}, & \text{on } \bar{X} = 0.
\end{cases}
\tag{5.35}
$$

This system is solved subject to the following far field conditions, acting as boundary conditions at the inlet of domain II and the outlet of domain III, obtained from matching the inner solutions to the solutions in the outer domain, via

$$
\bar{\boldsymbol{U}}^{(0)} \sim 6\bar{Z} \left(1 - \bar{Z} \right) f(T) \boldsymbol{e}_X \qquad \text{for } \bar{X} \to -\infty,
\tag{5.36}
$$

$$\bar{P}_P^{(1)} \sim \left(P_P^{(1)}(0,T) + \frac{\partial P_P^{(0)}(\epsilon\bar{X},T)}{\partial\epsilon}\Big|_{\epsilon=0} \right) \qquad \text{for } \bar{X} \to +\infty. \tag{5.37}$$

This problem is then solved numerically to obtain the leading order velocities fields $\bar{\boldsymbol{U}}^{(0)}$, $\bar{\boldsymbol{V}}^{(0)}$ and the first-order pressure fields $\bar{P}_F^{(1)}$, $\bar{P}_P^{(1)}$.

5.2.4. *Coupling conditions across the outer domains.* The analysis in the outer domains left us with six unknowns to be determined (three for the leading order problem and three for order $O(\epsilon)$ problem): $P_F^{00}(T)$ and $P_F^{10}(T)$ for the outer fluid domain and $P_P^{01}(T)$, $P_P^{11}(T)$, $\Sigma_{XX}'^{(0)}|_{X=0}(T)$ and $\Sigma_{XX}'^{(1)}|_{X=0}(T)$ for the outer poroelastic domain. To close the problem, we thus need six coupling conditions, imposed at $X = 0$, to relate the outer solutions in fluid domain I and the poroelastic domain IV. These effective coupling conditions are obtained using the solutions in the inner domains II and III and matching them with the outer solutions in domains I and IV.

From (5.32) we found that the pressure is constant across the inner domains, with $\bar{K}\bar{P}_F^{(0)} = \bar{P}_P^{(0)}$. Matching the inner solutions with the outer domains, we get $\bar{P}_P^{(0)} \sim P_P^{(0)}(0,T)$ for $\bar{X} \to +\infty$ and $\bar{P}_F^{(0)} \sim P_F^{(0)}(0,T)$ for $\bar{X} \to -\infty$. From (5.14a,b), $P_F^{(0)}(T) = P_F^{00}(T)$ so the coupling condition for the leading order pressures is

$$P_F^{00} = \frac{P_P^{(0)}(0,T)}{\bar{K}}. \tag{5.38}$$

At the order $O(\epsilon)$ the inner domains are governed by the Stokes-Darcy problem in (5.35); once $\bar{P}_F^{(1)}$ is computed throughout the inner fluid domain II, we can use the matching condition with the outer fluid domain $\bar{P}_F^{(1)} \sim P_F^{10} - 12\bar{X}f(T)$ for $\bar{X} \to -\infty$ to compute $P_F^{10}(T)$.

From problems (5.33) and (5.34) we see that the displacement in the inner domain is in the axial direction and is spatially homogeneous at both the leading and first order. Domain III is also stress free at these orders, and we can match the inner stress field with outer stress field for $\bar{X} \to \infty$ to obtain

$$\lim_{\bar{X}\to\infty} \bar{\Sigma}_{XX}'^{(0)} = 0 = \Sigma_{XX}'^{(0)}|_{X=0}, \quad \lim_{\bar{X}\to\infty} \bar{\Sigma}_{XZ}'^{(0)} = 0 = \Sigma_{XZ}'^{(0)}|_{X=0}, \tag{5.39}$$
$$\lim_{\bar{X}\to\infty} \bar{\Sigma}_{XX}'^{(1)} = 0 = \Sigma_{XX}'^{(1)}|_{X=0}, \quad \lim_{\bar{X}\to\infty} \bar{\Sigma}_{XZ}'^{(1)} = 0 = \Sigma_{XZ}'^{(1)}|_{X=0},$$

from which we obtain the unknowns $\Sigma_{XX}'^{(0)}|_{X=0}$ and $\Sigma_{XX}'^{(1)}|_{X=0}$ required for the equations (5.30) and (5.31).

To obtain the functions $P_P^{01}(T)$ and $P_P^{11}(T)$, we use a global conservation of mass argument [17]. First, we focus on the leading order and we refer to the problem for the velocities as shown in Fig. 5.3. In the inner domains, from (5.35), we know that $\nabla\cdot\bar{\boldsymbol{U}}^{(0)} = 0$ in region II and $\nabla\cdot\bar{\boldsymbol{V}}^{(0)} = 0$ in region III; applying the divergence theorem to the inner domains and using the boundary conditions for the normal velocities at $Z = 0, 1$ in (5.10), we can write

$$\int_0^1 \left(\bar{U}_X^{(0)} - \bar{V}_X^{(0)}\right)\big|_{\bar{X}=0}\mathrm{d}\zeta = \int_0^1 \lim_{\bar{X}\to-\infty} \bar{U}_X^{(0)}\mathrm{d}\zeta - \int_0^1 \lim_{\bar{X}\to\infty} \bar{V}_X^{(0)}\mathrm{d}\zeta. \tag{5.40}$$
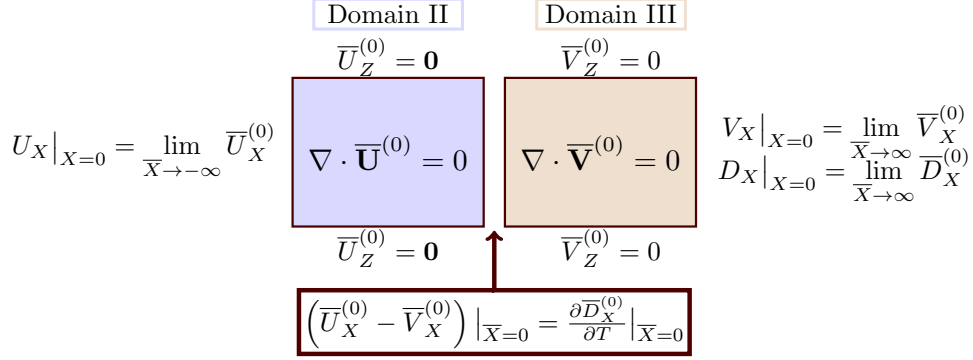
FIGURE 5.3. Leading order structure of the velocity fields in the inner domains II and III. Matching conditions with the outer solutions are shown on the left of domain II and on the right of domain III.

Employing the interface condition (5.11a) across domains II and III at leading order $\left(\bar{U}_X^{(0)} - \bar{V}_X^{(0)}\right)\big|_{\bar{X}=0} = \partial \bar{D}_X^0/\partial T\big|_{\bar{X}=0}$, and the matching conditions for the velocity field in the fluid domain, $\bar{U}_X^{(0)}\big|_{\bar{X}\to-\infty} = U_X^{(0)}\big|_{X=0}$, and for the velocity and displacement fields in the poroelastic domain, $\lim\limits_{\bar{X}\to\infty} \bar{V}_X^{(0)} = V_X^{(0)}\big|_{X=0}$ and $\bar{D}_X^{(0)}\big|_{\bar{X}=0} = \lim\limits_{\bar{X}\to\infty} \bar{D}_X^{(0)} = D_X^{(0)}\big|_{X=0}$, gives the following coupling condition for the outer I and IV domains

$$\int_0^1 U_X^{(0)}(X=0,T)\mathrm{d}\zeta = \int_0^1 \left(\frac{\partial D_X^{(0)}}{\partial T}\Big|_{X=0} + V_X^{(0)}(X=0,T)\right)\mathrm{d}\zeta, \qquad (5.41)$$

where we point out that the function $P_P^{01}(T)$ is in the expression of $V_X^{(0)}(X,T)$. Analogous arguments can be used at order $O(\epsilon)$ to obtain the function $P_P^{11}(T)$ using

$$\int_0^1 U_X^{(1)}(X=0,T)\mathrm{d}\zeta = \int_0^1 \left(\frac{\partial D_X^{(1)}}{\partial T}\Big|_{X=0} + V_X^{(1)}(X=0,T)\right)\mathrm{d}\zeta. \qquad (5.42)$$

5.2.5. *Solutions in the poroelastic domain IV.* Employing the coupling conditions (5.39), (5.41) and (5.42), we can state the full solution for the pressure, displacement and velocities fields in the poroelastic domain IV. At leading order, we obtain

$$P_P^{(0)}(X,T) = -f(T)\int_1^X \frac{1}{\mathcal{K}_0^{(0)}(\xi)}\mathrm{d}\xi + \int_1^X \frac{\partial A_D^{(0)}(\xi,T)}{\partial T}\frac{1}{\mathcal{K}_0^{(0)}(\xi)}\mathrm{d}\xi, \qquad (5.43a)$$

$$\mathbf{V}^{(0)}(X,T) = \left(f(T) - \frac{\partial A_D^{(0)}(X,T)}{\partial T}\right)\mathbf{e}_X, \qquad (5.43b)$$

$$\boldsymbol{D}^{(0)}(X,T) = A_D^{(0)}(X,T)\mathbf{e}_X, \qquad (5.43c)$$

with $A_D^{(0)}(X,T)$ given by the solution of (5.30). At leading order, the pressure, displacement and velocity fields do not depend on the transverse coordinate Z.

At first order, the solution is

$$P_P^{(1)}(X,T) = \int_1^X \frac{\partial A_D^{(1)}(\xi,T)}{\partial T} \frac{1}{\mathcal{K}_0^{(0)}(\xi)} \mathrm{d}\xi$$

$$+ \int_1^X \frac{1}{\mathcal{K}_0^{(0)}(\xi)} \left(-f(T) + \frac{\partial A_D^{(0)}(\xi,T)}{\partial T}\right) \left(\int_0^1 \frac{\mathcal{K}_0^{(1)}(\xi,\zeta)}{\mathcal{K}_0^{(0)}(\xi)} \mathrm{d}\zeta\right) \mathrm{d}\xi, \quad (5.44\text{a})$$

$$\mathbf{V}^{(1)}(X,Z,T) = \left(-\frac{\partial A_D^{(1)}}{\partial T} + \left(f(T) - \frac{\partial A_D^{(0)}}{\partial T}\right) \left(\frac{\mathcal{K}_0^{(1)}(X,Z)}{\mathcal{K}_0^{(0)}(X)} - \int_0^1 \frac{\mathcal{K}_0^{(1)}(X,Z)}{\mathcal{K}_0^{(0)}(X)} \mathrm{d}Z\right)\right) \mathbf{e}_X$$

$$+ \left[\int_0^Z \frac{\partial}{\partial X} \left(\left(-f(T) + \frac{\partial A_D^{(0)}(X,T)}{\partial T}\right) \frac{\mathcal{K}_0^{(1)}(X,\zeta)}{\mathcal{K}_0^{(0)}(X)}\right) \mathrm{d}\zeta \right.$$

$$\left. - Z \frac{\partial}{\partial X} \left(\left(-f(T) + \frac{\partial A_D^{(0)}(X,T)}{\partial T}\right) \int_0^Z \frac{\mathcal{K}_0^{(1)}(X,\zeta)}{\mathcal{K}_0^{(0)}(X)} \mathrm{d}\zeta\right)\right] \mathbf{e}_Z,$$

$$(5.44\text{b})$$

$$\boldsymbol{D}^{(1)}(X,Z,T) = A_D^{(1)}(X,T)\mathbf{e}_X + \frac{1}{2\mathcal{H}_0^{(0)} + \mathcal{N}_0^{(0)}} \left(Z \int_0^1 \mathcal{N}_0^{(1)} \mathrm{d}\zeta - \int_0^Z \mathcal{N}_0^{(0)} \mathrm{d}\zeta\right) \frac{\partial A_D^{(0)}}{\partial X} \mathbf{e}_Z,$$

$$(5.44\text{c})$$

with $A_D^{(1)}(X,T)$ given by the solution of (5.31). We see that the first-order correction to the pressure $P_P^{(1)}$ does not depend on Z, and only retains the X-dependence. The Darcy velocity and the displacement field, however, do vary in Z: specifically, this dependence is controlled by the expression of $\mathcal{K}_0^{(1)}$ for the former and by $\mathcal{H}_0^{(1)}$ for the latter.

5.3. Limiting cases.
Having determined analytical expressions for the flow and displacement in the outer domain IV, we now consider some limiting cases.

Steady flow. In the case where the driving upstream flow is steady ($f(T) = 1$) all the time derivatives appearing in the solutions (5.43) and (5.44) are zero. The solutions at leading order are then

$$P_P^{(0)}(X) = -\int_1^X \frac{1}{\mathcal{K}_0^{(0)}(\xi)} \mathrm{d}\xi, \quad (5.45\text{a})$$

$$\mathbf{V}^{(0)}(X) = \mathbf{e}_X, \quad (5.45\text{b})$$

$$\boldsymbol{D}^{(0)}(X) = \int_X^1 \left[\frac{1}{\left(2\mathcal{H}_0^{(0)}(\xi) + \mathcal{N}_0^{(0)}(\xi)\right)} \int_0^\xi \frac{1}{\mathcal{K}_0^{(0)}(\eta)} \mathrm{d}\eta\right] \mathrm{d}\xi \mathbf{e}_X. \quad (5.45\text{c})$$

while at order $O(\epsilon)$ we have

$$P_P^{(1)}(X) = -\int_1^X \frac{1}{\mathcal{K}_0^{(0)}(\xi)} \left(\int_0^1 \frac{\mathcal{K}_0^{(1)}(\xi,\zeta)}{\mathcal{K}_0^{(0)}(\xi)} \mathrm{d}\zeta\right) \mathrm{d}\xi, \quad (5.46\text{a})$$

$$\mathbf{V}^{(1)}(X,Z,T) = \left(\left(\frac{\mathcal{K}_0^{(1)}(X,Z)}{\mathcal{K}_0^{(0)}(X)} - \int_0^1 \frac{\mathcal{K}_0^{(1)}(X,Z)}{\mathcal{K}_0^{(0)}(X)} \mathrm{d}Z\right)\right) \mathbf{e}_X$$

$$+ \left[-\int_0^Z \frac{\partial}{\partial X}\left(\frac{\mathcal{K}_0^{(1)}(X,\zeta)}{\mathcal{K}_0^{(0)}(X)} \right) d\zeta + Z\frac{\partial}{\partial X}\left(\int_0^Z \frac{\mathcal{K}_0^{(1)}(X,\zeta)}{\mathcal{K}_0^{(0)}(X)} d\zeta \right) \right] \mathbf{e}_Z,$$
(5.46b)

$$\boldsymbol{D}^{(1)}(X) = \left[-\int_X^1 \left(\frac{1}{2\mathcal{H}_0^{(0)} + \mathcal{N}_0^{(0)}} \right) \left(\int_1^X \frac{1}{\mathcal{K}_0^{(0)}(\xi)} \left(\int_0^1 \frac{\mathcal{K}_0^{(1)}(\xi,\zeta)}{\mathcal{K}_0^{(0)}(\xi)} d\zeta \right) d\xi \right) d\xi \right.$$
$$\left. + \int_X^1 \left(\frac{\int_0^1 \left(2\mathcal{H}_0^{(1)} + \mathcal{N}_0^{(1)} \right) d\zeta}{\left(2\mathcal{H}_0^{(0)} + \mathcal{N}_0^{(0)} \right)^2} \int_0^\xi \frac{1}{\mathcal{K}_0^{(0)}} d\eta \right) d\xi \right] \mathbf{e}_X$$
$$- \frac{1}{\left(2\mathcal{H}_0^{(0)} + \mathcal{N}_0^{(0)} \right)^2} \int_0^X \frac{1}{\mathcal{K}_0^{(0)}} d\xi \left(Z\int_0^1 \mathcal{N}_0^{(1)} d\zeta - \int_0^Z \mathcal{N}_0^{(1)} d\zeta \right) \mathbf{e}_Z.$$
(5.46c)

In this regime, the deformation of the solid skeleton and the flow of the fluid phase decouple. Indeed, pressure and velocity are uniquely determined by the permeability function $\mathcal{K}_0$, while the elastic properties $\mathcal{H}_0$ and $\mathcal{N}_0$ only enter in the expression for displacement.

Rigid solid skeleton. Assuming a rigid solid skeleton implies $A_D^{(0)}, A_D^{(1)} \to 0$ and the the sets of solutions (5.43a), (5.43b) and (5.44a), (5.44b) can be simplified as

$$P_P^{(0)}(X,T) = -f(T)\int_1^X \frac{1}{\mathcal{K}_0^{(0)}(\xi)} d\xi,$$
(5.47a)

$$\mathbf{V}^{(0)}(X,T) = f(T)\mathbf{e}_X,$$
(5.47b)

and

$$P_P^{(1)}(X,T) = -f(T)\int_1^X \frac{1}{\mathcal{K}_0^{(0)}(\xi)} \left(\int_0^1 \frac{\mathcal{K}_0^{(1)}(\xi,\zeta)}{\mathcal{K}_0^{(0)}(\xi)} d\zeta \right) d\xi,$$
(5.48a)

$$\mathbf{V}^{(1)}(X,Z,T) = f(T)\left(\frac{\mathcal{K}_0^{(1)}(X,Z)}{\mathcal{K}_0^{(0)}(X)} - \int_0^1 \frac{\mathcal{K}_0^{(1)}(X,Z)}{\mathcal{K}_0^{(0)}(X)} dZ \right) \mathbf{e}_X$$
$$+ f(T)\left[-\int_0^Z \frac{\partial}{\partial X}\left(\frac{\mathcal{K}_0^{(1)}(X,\zeta)}{\mathcal{K}_0^{(0)}(X)} \right) d\zeta + Z\frac{\partial}{\partial X}\left(\int_0^Z \frac{\mathcal{K}_0^{(1)}(X,\zeta)}{\mathcal{K}_0^{(0)}(X)} d\zeta \right) \right] \mathbf{e}_Z,$$
(5.48b)

showing that any temporal dynamics for the pressure and the Darcy velocity, at both orders in the rigid porous domain, is proportional to the imposed $f(T)$ at the inlet.

Homogeneous material properties. In the limit of homogeneous material properties we can write $\mathcal{K}_0(X,Z) = \bar{\mathcal{K}}_0$, $\mathcal{H}_0(X,Z) = \bar{\mathcal{H}}_0$ and $\mathcal{N}_0(X,Z) = \bar{\mathcal{N}}_0$. At $O(1)$, the solutions (5.43) simplify as

$$P_P^{(0)}(X,T) = \frac{1}{\bar{\mathcal{K}}_0}\left(-f(T)(X-1) + \int_1^X \frac{\partial A_D^{(0)}(\xi,T)}{\partial T} d\xi \right),$$
(5.49a)

$$\mathbf{V}^{(0)}(X,T) = \left(f(T) - \frac{\partial A_D^{(0)}(X,T)}{\partial T} \right) \mathbf{e}_X,$$
(5.49b)

$$\boldsymbol{D}^{(0)}(X,T) = A_D^{(0)}(X,T)\mathbf{e}_X,$$
(5.49c)

with $A_D^{(0)}(X,T)$ being the solution of the ODE (5.30) with constant elastic parameters. At the order $O(\epsilon)$, the solutions (5.44a), (5.44b) and (5.44c) rewrite as

$$P_P^{(1)}(X,T) = \frac{1}{\bar{K}\bar{\mathcal{K}}_0} \int_1^X \frac{\partial A_D^{(1)}(\xi,T)}{\partial T} d\xi, \tag{5.50a}$$

$$\mathbf{V}^{(1)}(X,Z,T) = \mathbf{0}, \tag{5.50b}$$

$$\boldsymbol{D}^{(1)}(X,T) = A_D^{(1)}(X,T)\mathbf{e}_X, \tag{5.50c}$$

with $A_D^{(1)}(X,T)$ now solution of

$$- P_P^1(X=0,T) = \left(2\bar{\mathcal{H}}_0 + \bar{\mathcal{N}}_0\right)\frac{\partial A_D^{(1)}}{\partial X} - P_P^{(1)}. \tag{5.51}$$

In the homogeneous case, we lose any dependence of the solutions on the axial coordinate, and the correction to the Darcy velocity $\mathbf{V}^{(1)}(X,Z,T)$ is zero.

6. NUMERICAL SOLUTION

We now solve the governing equations numerically using the finite element approach given in §3. We specify the form of the material properties motivated by the following observation. From (5.43a), (5.43b) and (5.43c) we see that, at leading order, everything depends only on X while, from (5.44b), we see that a cross term of the type (XZ) in the permeability function is required to have a non zero $V_Z^{(1)}$. We therefore prescribe the following functional forms for the material properties

$$\mathcal{K}_0 = 1.5 + 4.2X + \epsilon 1.2XZ, \quad \mathcal{H}_0 = 1 - 0.2X - \epsilon 0.1XZ, \quad \mathcal{N}_0 = 4 - 0.1X - \epsilon 0.1XZ. \tag{6.1}$$

Note that for simplicity and illustrative purposes, we prescribe the material properties to depend directly on the spatial coordinates X and Z, rather than prescribing a spatially-varying porosity field and giving a constitutive relationship between the material properties and the porosity. We also set $\bar{K} = 0.06$ and the aspect ratio $\epsilon = 0.05$.

The problem implemented in the finite element method presented in §3 is dimensional and, for our validation, we set the parameters with numerical values equal to $h = \epsilon$, $l = 1$, $\mu_f = 1$, $\mu_{s,0} = 800000$, $\gamma = 0$ and $\kappa_0 = \bar{K}\epsilon^2 = 0.00015$, and having consistent units of measure. We consider flows driven by either a steady or a oscillatory upstream velocity profiles: in the latter case, we consider the case where the dimensional pulsation of the velocity profile is the inverse of the characteristic time of the problem.

We start by comparing the numerical and analytical predictions for the dimensionless velocities ((5.45b) and (5.46b)), pressures ((5.45a) and (5.46a)) and displacements ((5.45c) and (5.46c)) in the steady case ($f(T) = 1$). In Fig. 6.1 we plot the pressure, axial flow and axial displacement fields in the coupled Stokes flow-poroelastic domain, where the red and blue curves refer quantities to the outer Stokes flow (I) and poroelastic domain IV, respectively, and the black curves to the finite element numerical results. All curves obtained within the lubrication limit are up to $O(\epsilon)$ except the pressure in the fluid domain that requires the solution of the inner problem in (5.35) (not solved here numerically). The agreement between the analytical and numerical predictions is excellent, and increases with the addition of the $O(\epsilon)$ correction to the leading-order analytical solution.
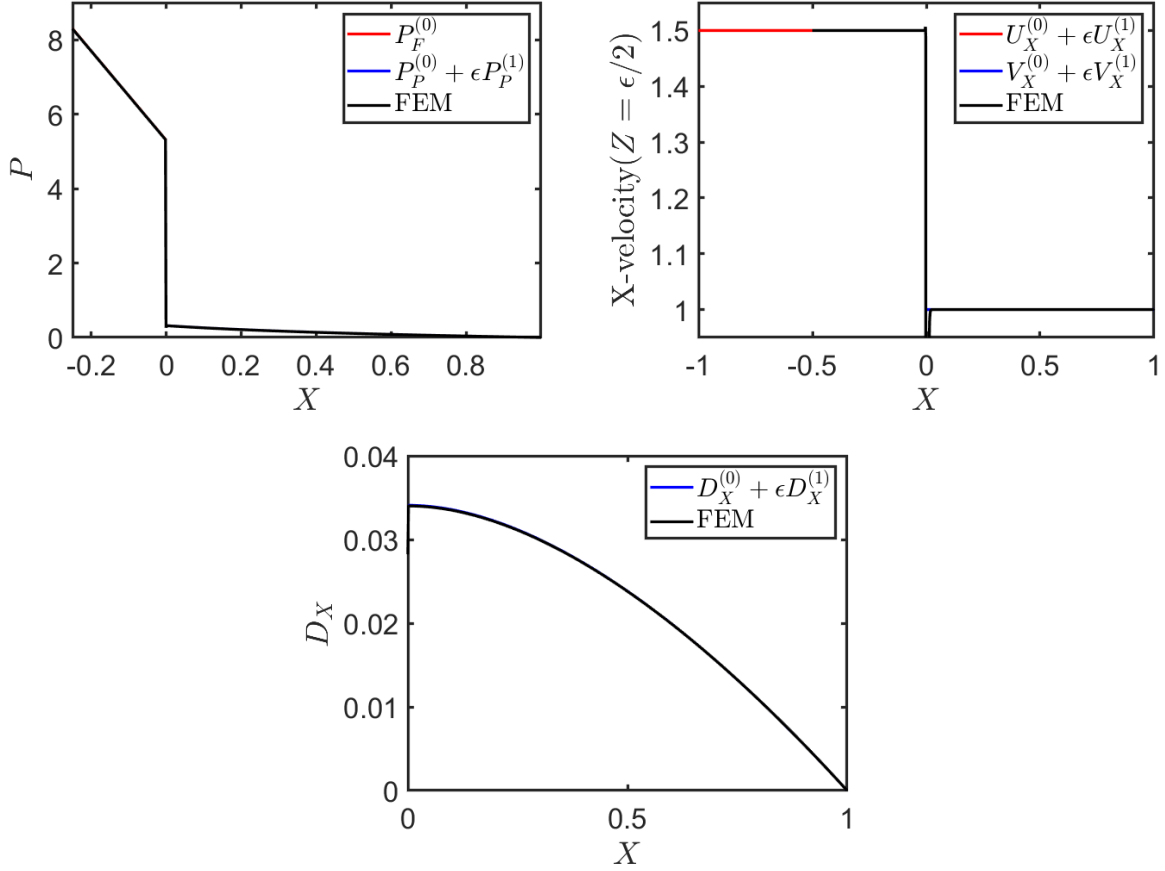
FIGURE 6.1. Comparison between the lubrication limit and the finite element computations in terms of (top left) pressure field, (top right) axial velocity field and (bottom) axial displacement field in the porous domain. Red and blue curves refer to the outer fluid and porous domains, respectively, and the black curves to finite element solutions. The agreement of the numerical solution is very good; as an example to make the overlap with the analytical solution clearer, in the top right panel we plot the black curve from the finite element results, not covering the entire domain $X \in [-1, 1]$.

The transverse Darcy velocity V_Z and the transverse displacement D_Z in domain IV is nonzero at $O(\epsilon)$ (see the analytical solutions (5.45c),(5.45b), (5.46c) and (5.46b)). In Fig. 6.2 (top row) we compare the analytical prediction and the numerical result for those two quantities at three values of the transverse coordinates $Z = [0.1, 0.25, 0.5]$. While the transverse coordinate is decreasing, moving from the centre-line to the lateral boundary, the numerical result follows the same trend that we see in the analytical solutions. To quantify the quantitative discrepancy in term of the numerical values, in Fig. 6.2 (bottom row) we present the error (as difference between the analytical prediction and the numerical result) of the quantities presented in 6.2 (top row). We expect the errors to be of $O(\epsilon^2)$ and this comparison reveals a good agreement for both the velocity and the displacement fields. The errors increase when moving closer to the interfaces, $X = 0$ that is the fluid-poroelastic coupling and $X = 1$ that is the outlet.
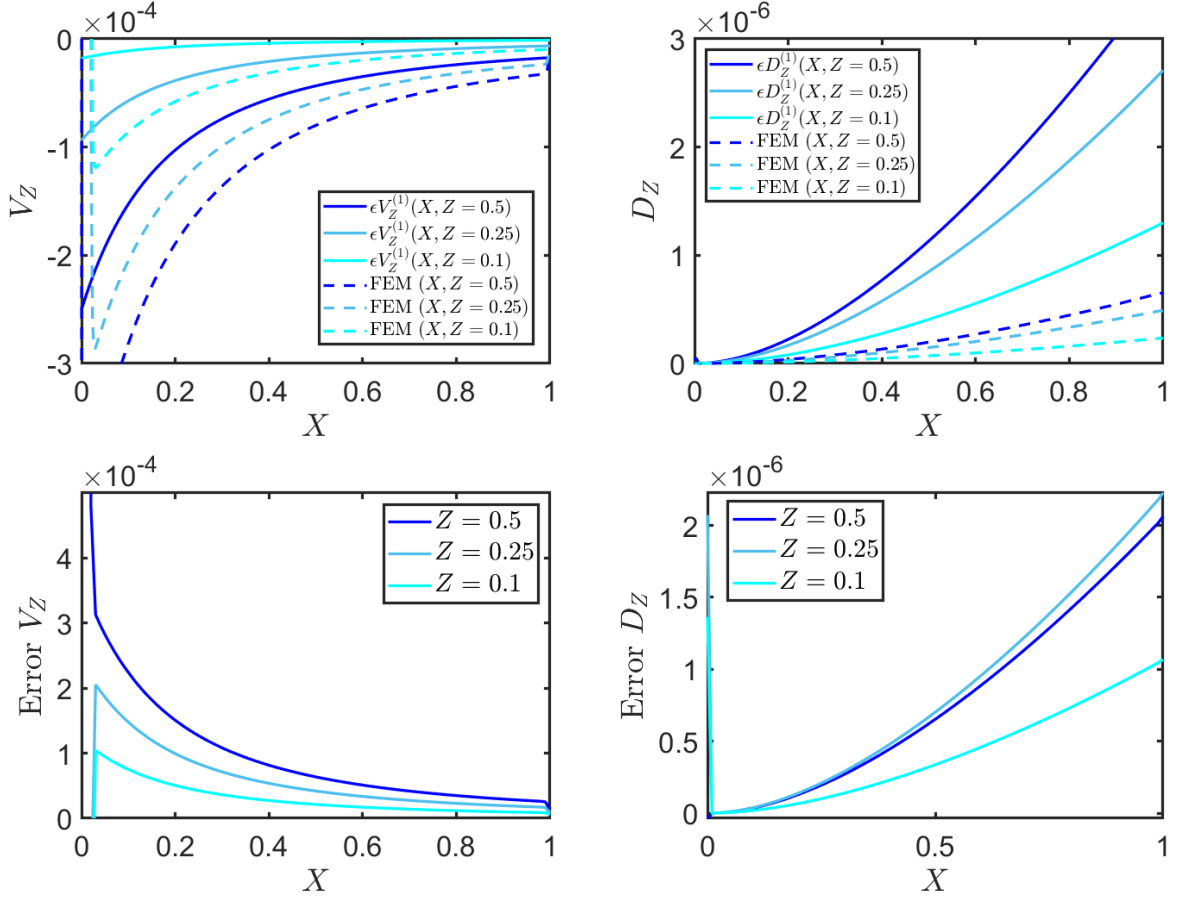
FIGURE 6.2. (top row) Comparison between the analytical prediction and finite element result for the transverse Darcy velocity (left) and the transverse displacement (right). Transverse positions indicated by dark blue ($Z = 0.5$), mid blue ($Z = 0.25$) and light blue ($Z = 0.1$). Continuous lines correspond to the analytical solutions, and dashed lines refer to the finite element computations. (bottom row) Difference along the longitudinal coordinate X between the analytical prediction and finite element result for the transverse Darcy velocity (left) and the transverse displacement (right) at the same three Z coordinates.

In Fig. 6.3 we present the comparison in the oscillatory regime ($f(T) = \cos(T)$) in term of the the pressure field P_P and the displacement D_X in the poroelastic domain IV. For both these two quantities we present the modulus and the phase shift with respect to the forcing $f(T)$ computed at the centre-line $Z = 0.5$ and for different coordinates X; the continuous lines refer to the solutions in the lubrication limit and the empty circles to the finite element simulations. The X dependence of modulus is, as expected, the same as obtained in the steady case (the material parameters are kept the same). However, although we do not consider inertia in our modelling, the phase shift shows that both the quantities are delayed with respect to $F(T)$ and this is due to the fluid-elastic coupling present in domain IV.
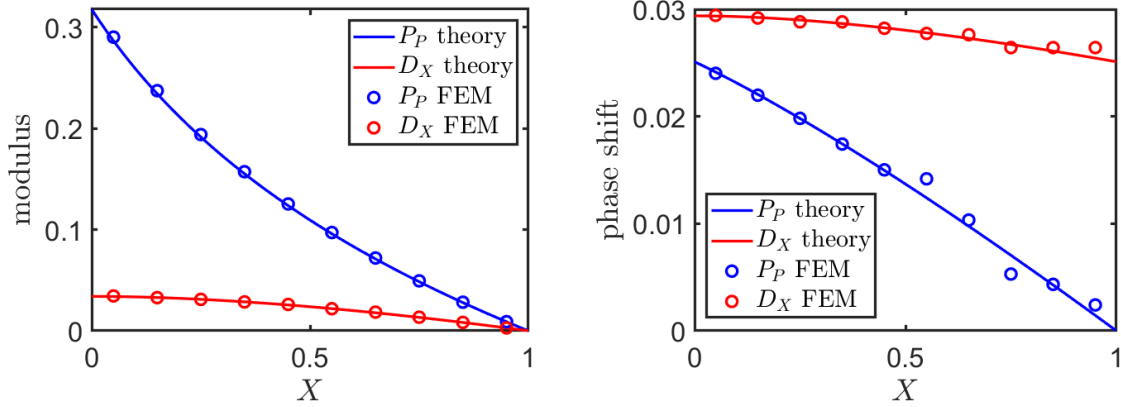
FIGURE 6.3.   Comparison between the oscillatory solution from the lubrication theory and the solution from the finite element simulations in term of modulus (left) and phase shift (right) of the pressure P_P (blue) and the longitudinal displacement D_X (red). Data shown here refer to centre-line $Z = 0.5$. Curves are the theoretical solutions and markers are the results from the finite element simulations.

7. CONCLUDING REMARKS

In this work we investigate the mechanics of a single-phase fluid-poroelastic system, coupled via appropriate interfacial conditions. In the fluid domain we assume a Newtonian incompressible fluid while the linear poroelastic domain has an inhomogeneous porosity that induces heterogeneity of the permeability and the Lamé parameters, eventually imposing their functional dependence on space.

The governing equations for the poroelastic domain in the small strain regime are derived from the nonlinear biphasic mixture theory. In the linearised formulation, the inhomogeneity enters the conservation equations only through the coefficients of the material properties. However, as heterogeneity modifies the variation of the porosity, a dependence on its gradient also appears when computing θ_1.

We consider the scenario where the characteristic time scale in the poroelastic domain ensures that the Darcy and solid skeleton velocities are comparable. As a consequence, we identify two dimensionless parameters, K_n and U_n.

Once the aspect ratio $\epsilon = a/L \ll 1$ of the two-dimensional channel is selected as a small parameter, we perform the asymptotic analysis presented in §4. In the lubrication limit, we can identify four zones within this geometrical configuration. The outer domains I (fluid) and IV (porous), where the mechanics depends on the interface via the derived coupling conditions in §5.2.4; the inner domains II (fluid) and III (porous), where the interface is the major effect in governing the flow behaviour.

In the outer domain I, we recover the analysis in [17] applied to our specific conditions imposed at the inlet. The driving flow in our setting is this prescribed upstream velocity profiles. In the outer domain IV we derive the governing equations up to the order $O(\epsilon)$ and obtain the corresponding solutions for the displacement field, the Darcy velocity and the pressure field. Employing the interfacial conditions, we show that the solutions in the

outer problem at leading order can be fully computed once the ODE (5.30) is solved. At order $O(\epsilon)$, instead, to compute the full solutions we do require both the solution of the ODE (5.31) and to know the function $P_F^{10}(T)$, available only when the inner Stokes-Darcy problem is solved. The two ODEs are the coupling conditions that we propose to couple domain I and domain IV, in terms of its solid effective elastic behaviour.

In the steady case, the elastic part of the poroelastic domain is decoupled from the fluid flow. In such a regime we can solve the ODEs (5.30) and (5.31) in closed form and write the solution for the pressure field, the Darcy velocity and the displacement field up to order $O(\epsilon)$ in terms of the functions that describe the material heterogeneity. In the case of a porous domain with a rigid solid skeleton, all the fields have the same temporal behaviour as the imposed forcing at the inlet $f(T)$: one of the effects of the deformability of the solid phase is thus to modulates the temporal dynamics of the pressures and velocities. The inhomogeneity in the material properties, instead, introduces a dependence on the transversal coordinate Z on both the first-order transversal velocity and displacement, otherwise lost in the case of homogeneous materials.

To investigate the inner domains II and III we consider the effect of the interface through the equations in (5.11). Interestingly, for the inner problem, the elastic and flow subproblems are decoupled, even in the transient case and up to the order $O(\epsilon)$. We find that the stress tensors at both leading order $\bar{\boldsymbol{\Sigma}}'^{(0)}$ and first-order $\bar{\boldsymbol{\Sigma}}'^{(1)}$ are divergence free, with no traction applied at the interface. Thus the poroelastic region III undergoes a rigid body motion of a constant displacement fixed by the outer domain IV. As a consequence, the fluid flow within the pores is regulated via a coupling between a Stokes domain and a Darcy domain with constant permeability, which is a much easier problem to solve numerically compared to the original Biot-Stokes system.

The finite element formulation that we present here rewrites the problem in the porous domain using the displacement, the fluid pressure, and the total pressure. The main advantage of this approach is to use a unique finite element discretisation that is stable in both the fluid domain and the porous domain, without the need of Lagrange multipliers for the imposition of interfacial conditions. Also, the stability and convergence of the method remain robust in the limits of very low permeability and of nearly effective incompressibility. The validity of the finite element model is tested against the solution obtained in the asymptotic limit and agreement is shown in §6.

Natural extensions of the present work are towards the analysis of the nonlinear case where large deformations are present. Moreover the effect of the interface can be investigated in a more general setting, studying how the description proposed here in the two-dimensional Cartesian setting can be generalised to interfaces of any three dimensional shapes. The finite element model presented here can be used to investigate realistic geometries, as in channels with $O(1)$ thickness where analytical solutions are more difficult to obtain, or specific biological applications, as the fluid drainage that happens in the eye or in blood vessels, to obtain insights on the mechanics of fluid - poroelastic systems in both the bulk and the interface regions.

APPENDIX A. DERIVATION OF THE SOLUTION IN THE OUTER FLUID DOMAIN I

Using the expansion proposed in (5.5) into the governing equations in the fluid domain (5.3), we obtain

$$\left(\frac{\partial U_X^{(0)}}{\partial Z^2} - \frac{\partial P_F^{(0)}}{\partial X}\right) + \epsilon\left(\frac{\partial U_X^{(1)}}{\partial Z^2} - \frac{\partial P_F^{(1)}}{\partial X}\right) + O(\epsilon^2) = 0, \tag{A.1}$$

$$\left(\frac{\partial P_F^{(0)}}{\partial Z}\right) + \epsilon\left(\frac{\partial P_F^{(1)}}{\partial Z}\right) + O(\epsilon^2) = 0, \tag{A.2}$$

$$\left(\frac{\partial U_X^{(0)}}{\partial X} + \frac{\partial U_Z^{(0)}}{\partial Z}\right) + \epsilon\left(\frac{\partial U_X^{(1)}}{\partial X} + \frac{\partial U_Z^{(1)}}{\partial Z}\right) + O(\epsilon^2) = 0. \tag{A.3}$$

At the leading order, from (A.2) we obtain

$$P_F^{(0)} = P_F^{(0)}(X, T), \tag{A.4}$$

and, from (A.1),

$$U_X^{(0)} = \frac{Z^2}{2}\frac{\partial P_F^{(0)}}{\partial X} + Z U_X^{01}(X, T) + U_X^{00}(X, T), \tag{A.5}$$

with $U_X^{00}(X, T) = 0$ and $U_X^{01}(X, T) = -\left(\partial P_F^{(0)}/\partial X\right)/2$ when imposing $U_X^{(0)}(Z = 0, 1) = 0$ from the no-slip condition (5.4a). From (A.3) we can thus obtain the leading velocity along Z as

$$U_Z^{(0)} = U_Z^{00}(X, T) - \frac{1}{2}\left(\frac{Z^3}{3} - \frac{Z^2}{2}\right)\frac{\partial^2 P}{\partial X^2}. \tag{A.6}$$

Using the no-slip condition $U_Z^{(0)}(Z = 0) = 0$, we get $U_Z^{00}(X, T) = 0$ while from $U_Z^{(0)}(Z = 1) = 0$ we have the equation for the pressure that decay linearly with X as

$$P_F^{(0)} = P_F^{00}(T) + P_F^{01}(T)X, \tag{A.7}$$

that in turn gives

$$U_X^{(0)} = \frac{1}{2}P_F^{01}\left(Z^2 - Z\right). \tag{A.8}$$

At the leading order, the condition on the imposed velocity at the inlet (5.4d) reduces to be

$$\int_0^1 U_X^{(0)}\mathrm{d}Z = f(T), \tag{A.9}$$

and we get $P_F^{01}(T) = -12f(T)$.

At the order $O(\epsilon)$, the governing equations are formally equal to what we got at the leading order once using the second term in the expansion for the variables. We thus obtain

$$P_F^{(1)} = P_F^{10}(T) + P_F^{11}(T)X, \qquad U_X^{(1)} = \frac{1}{2}P_F^{11}(T)\left(Z^2 - Z\right), \qquad U_Z^{(1)} = 0, \tag{A.10}$$

with the condition on the imposed velocity at the inlet (5.4d) at the first order to be

$$\epsilon^2 \int_0^1 U_X^{(1)} \mathrm{d}Z = 0. \tag{A.11}$$

From this we obtain $P_F^{11}(T) = 0$ and thus we recover the expressions presented in (5.14a,b) and (5.14c,d).

References

[1] S. Badia, A. Quaini and A. Quarteroni, Coupling Biot and Navier-Stokes equations for modelling fluid-poroelastic media interaction, *J. Comput. Phys.* **228** (2009) 7986 - 8014.

[2] A.J. El-Haj, S.L. Minter, S.C. Rawlinson, R. Suswillo and L.E. Lanyon, Cellular responses to mechanical loading in vitro, *J. Bone and Min. Res.* **5** (1990) 923 - 32.

[3] P. Thomen, J. Robert, A. Monmeyran, A.F. Bitbol, C. Douarche and N. Henry, Bacterial biofilm under flow: First a physical struggle to stay, then a matter of breathing, *PLoS ONE* **12** (2017) e0175197.

[4] I. Ambartsumyan, E. Khattatov, T. Nguyen and I. Yotov, Flow and transport in fractured poroelastic media, *GEM Int. J. Geomath.* **10** (2019) 11.

[5] O. Coussy, *Poromechanics.* (John Wiley & Sons Ltd, Chichester, UK 2004).

[6] S.C. Cowin and S.B. Doty, *Tissue Mechanics.* (Springer-Verlag, New York, USA 2007).

[7] K. Terzaghi, Principles of Soil Mechanics: I—Phenomena of Cohesion of Clays, *Engineering News-Record* **95** (1925) 742 - 746.

[8] M.A. Biot, General theory of three-dimensional consolidation, *J. Appl. Phys.* **12** (1941) 155 - 164.

[9] G.E. Lang, D. Vella, S.L. Waters and A. Goriely, Mathematical modelling of blood-brain barrier failure and oedema, *Math. Med. Biol.* **34** (2016) 391 - 414.

[10] G.A. Ateshian and J.A. Weiss, Anisotropic hydraulic permeability under finite deformation, *J. Biomech. Eng.* **132** (2010) 111004(7).

[11] S. Federico and W. Herzog, On the anisotropy and inhomogeneity of permeability in articular cartilage, *Biomech. Model. Mechanobiol.* **7** (2007) 367 - 378.

[12] B. Nedjar, Formulation of a nonlinear porosity law for fully saturated porous media at finite strains, *J. Mech. Phys. Solids* **61** (2013) 537 - 556.

[13] C.W. MacMinn, E.R Dufresne and J.S Wettlaufer, Large deformations of a soft porous material, *Phys. Rev. Applied* **5** (2016) 044020(30).

[14] C.C. Mei, J.I Auriault and F.J. Ursell, Mechanics of heterogeneous porous media with several spatial scales, *Proc. Royal Soc. London A* **426** (1997) 391 - 423.

[15] A.E. Sáez, C.J Otero and I. Rusinek, The effective homogeneous behavior of heterogeneous porous media, *Transport Porous Med.* **4** (1989) 213 - 238.

[16] R.E. Showalter, Poroelastic Filtration Coupled to Stokes Flow, pp. 229 - 241 , in O. Imanuvilov, G. Leugering, R. Triggiani and B.Y. Zhang, *Control Theory of Partial Differential Equations - Lecture Notes in Pure and Applied Mathematics vol. 242* (Chapman & Hall, Boca Raton, 2005).

[17] M. Dalwadi, S.J. Chapman, S.L. Waters and J. Oliver, On the boundary layer structure near a highly permeable porous interface, *J. Fluid Mech.* **798** (2016) 88 - 139.

[18] L.M. De Oliveira Vilaca, B. Gómez-Vargas, S. Kumar, R. Ruiz-Baier and N. Verma, Stability analysis for a new model of multi-species convection-diffusion-reaction in poroelastic tissue, *Appl. Math. Model.* **84** (2020) 425 - 446.

[19] C. Yu, K. Malakpoor and J.M. Huyghe, A mixed hybrid finite element framework for the simulation of swelling ionized hydrogels, *Comput. Mech.* **63** (2019) 835 - 852.

[20] R.T. Mauck, C.T. Hung and G.A. Ateshian, Modelling of neutral solute transport in a dynamically loaded porous permeable gel: implications for articular cartilage biosynthesis and tissue engineering, *J. Biomech. Eng.* **125** (2003) 602 - 614.

[21] M. Bukač, I. Yotov, R. Zakerzadeh and P. Zunino, Partitioning strategies for the interaction of a fluid with a poroelastic material based on a Nitsche's coupling approach, *Comput. Methods Appl. Mech. Eng.* **292** (2015) 138 - 170.

[22] I. Ambartsumyan, E. Khattatov, I. Yotov and P. Zunino, A Lagrange multiplier method for a Stokes–Biot fluid–poroelastic structure interaction model, *Numer. Math.* **140** (2018) 513 - 553.

[23] C. Ager, B. Schott, M. Winter and W.A. Wall, A Nitsche-based cut finite element method for the coupling of incompressible fluid flow with poroelasticity, *Comput. Methods Appl. Mech. Eng.* **351** (2019) 253 - 280.

[24] J. Lee, K.A. Mardal and R. Winther, Parameter-robust discretization and preconditioning of Biot's consolidation model, *SIAM J. Sci. Comput.* **9** (2017) A1 - A24.

[25] R. Oyarzúa and R. Ruiz-Baier, Locking-free finite element methods for poroelasticity, *SIAM J. Numer. Anal.* **54** (2016) 2951 - 2973.

[26] L. Preziosi and A. Farina, On Darcy's law for growing porous media, *Int. J. Nonlin. Mech.* **37** (2002) 485 - 491.

[27] B.W. Thompson, Secondary flow in a Hele-Shaw cell, *J. Fluid Mech.* **31** (1968) 379 - 395.

[28] M. Serpilli, Classical and higher order interface conditions in poroelasticity, *Ann. Solid Struct. Mech.* **11** (2019) 1 - 10.

[29] M.A. Murad, J.N. Guerreiro and A.F.D. Loula, Micromechanical computational modeling of secondary consolidation and hereditary creep in soils, *Comput. Methods Appl. Mech. Eng.* **190** (2001) 1985 - 2016.

[30] T. Karper, K.A. Mardal and R. Winther, Unified finite element discretizations of coupled Darcy–Stokes flow, *Numer. Methods Partial Differ. Equ.* **25** (2009) 311 - 326.

[31] M.S. Alnæs, J. Blechta, J. Hake, A. Johansson, B. Kehlet, A. Logg, C. Richardson, J. Ring, M.E. Rognes and G.N. Wells, The FEniCS Project Version 1.5, *Arch. Num. Soft.* **100** (2015) 9 - 23.

Mathematical Institute, University of Oxford, Radcliffe Observatory Quarter, Woodstock road, OX26GG Oxford, UK. Present address: Department of Engineering Mathematics, University of Bristol, BS8 1TW,Bristol, UK

Mathematical Institute, University of Oxford, Radcliffe Observatory Quarter, Woodstock road, OX26GG Oxford, UK. Present address: School of Mathematical Sciences, Monash University, 9 Rainforest Walk, Melbourne 3800 VIC, Australia

Mathematical Institute, University of Oxford, Radcliffe Observatory Quarter, Woodstock road, OX26GG Oxford, UK